



HAL
open science

State of the science in reconciling top-down and bottom-up approaches for terrestrial CO₂ budget

Masayuki Kondo, Prabir Patra, Stephen Sitch, Pierre Friedlingstein, Benjamin Poulter, Frederic Chevallier, Philippe Ciais, Josep Canadell, Ana Bastos, Ronny Lauerwald, et al.

► To cite this version:

Masayuki Kondo, Prabir Patra, Stephen Sitch, Pierre Friedlingstein, Benjamin Poulter, et al.. State of the science in reconciling top-down and bottom-up approaches for terrestrial CO₂ budget. *Global Change Biology*, 2020, 26 (3), pp.1068-1084. 10.1111/GCB.14917 . hal-02957731

HAL Id: hal-02957731

<https://hal.science/hal-02957731>

Submitted on 16 Jun 2021

HAL is a multi-disciplinary open access archive for the deposit and dissemination of scientific research documents, whether they are published or not. The documents may come from teaching and research institutions in France or abroad, or from public or private research centers.

L'archive ouverte pluridisciplinaire **HAL**, est destinée au dépôt et à la diffusion de documents scientifiques de niveau recherche, publiés ou non, émanant des établissements d'enseignement et de recherche français ou étrangers, des laboratoires publics ou privés.

1
2 PROF. MASAYUKI KONDO (Orcid ID : 0000-0001-5466-4847)
3 DR. BENJAMIN POULTER (Orcid ID : 0000-0002-9493-8600)
4 DR. VANESSA HAVERD (Orcid ID : 0000-0003-4359-5895)
5 DR. ATUL JAIN (Orcid ID : 0000-0002-4051-3228)
6 DR. ETSUSHI KATO (Orcid ID : 0000-0001-8814-804X)
7 DR. MARKUS KAUTZ (Orcid ID : 0000-0001-8763-3262)
8 DR. RACHEL M. LAW (Orcid ID : 0000-0002-7346-0927)
9 DR. DANICA LOMBARDOZZI (Orcid ID : 0000-0003-3557-7929)
10 DR. DAN ZHU (Orcid ID : 0000-0002-5857-1899)

11
12
13
14
15

Article type : Opinion

16 Prof. MASAYUKI KONDO (Orcid ID: 0000-0001-5466-4847)
17 Article type: Opinion

18 **State of the science in reconciling top-down and bottom-up** 19 **approaches for terrestrial CO₂ budget**

20 **Running Title:** On reconciliation of CO₂ budgets

21

22 Masayuki Kondo^{1,*}, Prabir K. Patra^{1,2}, Stephen Sitch³, Pierre Friedlingstein⁴, Benjamin Poulter⁵,
23 Frederic Chevallier⁶, Philippe Ciais⁶, Josep G. Canadell⁷, Ana Bastos⁸, Ronny Lauerwald⁹, Leonardo
24 Calle¹⁰, Kazuhito Ichii^{1,11}, Peter Anthoni¹², Almut Arneth¹², Vanessa Haverd¹³, Atul K. Jain¹⁴, Etsushi
25 Kato¹⁵, Markus Kautz^{12, 16}, Rachel M. Law¹⁷, Sebastian Lienert¹⁸, Danica Lombardozzi¹⁹, Takashi
26 Maki²⁰, Takashi Nakamura²¹, Philippe Peylin⁶, Christian Rödenbeck²², Zhuravlev Ruslan²³, Tazu
27 Saeki¹¹, Hanqin Tian²⁴, Dan Zhu⁶, Tilo Ziehn¹⁷

28

29 ¹Center for Environmental Remote Sensing, Chiba University, Chiba 263-8522, Japan

This is the author manuscript accepted for publication and has undergone full peer review but has not been through the copyediting, typesetting, pagination and proofreading process, which may lead to differences between this version and the [Version of Record](#). Please cite this article as [doi: 10.1111/GCB.14917](https://doi.org/10.1111/GCB.14917)

This article is protected by copyright. All rights reserved

30 ²Department of Environmental Geochemical Cycle Research, Japan Agency for Marine–Earth Science
31 and Technology, Yokohama 236-0001, Japan

32 ³College of Life and Environmental Sciences, University of Exeter, Exeter EX4 4QF, UK

33 ⁴College of Engineering, Mathematics and Physical Sciences, University of Exeter, Exeter EX4 4QF,
34 UK

35 ⁵National Aeronautics and Space Administration Goddard Space Flight Center, Biospheric Science
36 Laboratory, Greenbelt, MD 20771, USA

37 ⁶Laboratoire des Sciences du Climat et de l'Environnement, Institut Pierre Simon Laplace, 91191 Gif-
38 sur-Yvette, France

39 ⁷Global Carbon Project, Commonwealth Scientific and Industrial Research Organisation–Oceans and
40 Atmosphere, Canberra, ACT 2601, Australia

41 ⁸Department of Geography, Ludwig–Maximilians University of Munich, 80333 Munich, Germany

42 ⁹Université Libre de Bruxelles, 1050 Bruxelles, Belgium

43 ¹⁰W.A. Franke College of Forestry & Conservation, University of Montana, Missoula, MT 59812, USA

44 ¹¹Center for Global Environmental Research, National Institute for Environmental Studies, Tsukuba
45 305-8506, Japan

46 ¹²Institute of Meteorology and Climate Research/Atmospheric Environmental Research, Karlsruhe
47 Institute of Technology, 82467 Garmisch–Partenkirchen, Germany

48 ¹³Commonwealth Scientific and Industrial Research Organisation–Oceans and Atmosphere, Canberra,
49 ACT 2601, Australia

50 ¹⁴Department of Atmospheric Sciences, University of Illinois at Urbana–Champaign, Urbana, IL 61801,
51 USA

52 ¹⁵Institute of Applied Energy, Tokyo, 105-0003, Japan

53 ¹⁶Department of Forest Health, Forest Research Institute Baden–Württemberg, 79100 Freiburg, Germany

54 ¹⁷Commonwealth Scientific and Industrial Research Organisation–Oceans and Atmosphere, Aspendale,
55 VIC, Australia

56 ¹⁸Climate and Environmental Physics, Physics Institute and Oeschger Centre for Climate Change
57 Research, University of Bern, Bern, Switzerland

58 ¹⁹Climate and Global Dynamics, National Center for Atmospheric Research, Boulder, CO 80305, USA

59 ²⁰Meteorological Research Institute, Tsukuba 305-0052, Japan

60 ²¹Japan Meteorological Agency, Tokyo 100-8122, Japan

61 ²²Max Planck Institute for Biogeochemistry, 07745 Jena, Germany

62 ²³Central Aerological Observatory of Russian Hydromet Service, 141700, Russia

63 ²⁴International Center for Climate and Global Change Research, School of Forestry and Wildlife
64 Sciences, Auburn University, Auburn, AL 36849, USA

65

66 ***Correspondence:**

67 Masayuki Kondo

68 Center for Environmental Remote Sensing (CEReS), Chiba University

69 1-33 Yayoi-cho, Inage-ku, Chiba 263-8522, Japan

70 Tel/Fax: +81-43-290-3860

71 E-mail:

Mkondo@chiba-u.jp

Author Manuscript

73 **Abstract**

74 Robust estimates of CO₂ budget, CO₂ exchanged between the atmosphere and terrestrial biosphere, are
75 necessary to better understand the role of the terrestrial biosphere in mitigating anthropogenic CO₂
76 emissions. Over the past decade, this field of research has advanced through understanding of the
77 differences and similarities of two fundamentally different approaches: "top-down" atmospheric
78 inversions and "bottom-up" biosphere models. Since the first studies were undertaken, these approaches
79 have shown an increasing level of agreement, but disagreements in some regions still persist, in part
80 because they do not estimate the same quantity of atmosphere-biosphere CO₂ exchange. Here we
81 conducted a thorough comparison of CO₂ budgets at multiple scales and from multiple methods to
82 assess the current state of the science in estimating CO₂ budgets. Our set of atmospheric inversions and
83 biosphere models, which were adjusted for a consistent flux definition, showed a high level of
84 agreement for global and hemispheric CO₂ budgets in the 2000s. Regionally, improved agreement in
85 CO₂ budgets was notable for North America and Southeast Asia. However, large gaps between the two
86 methods remained in East Asia and South America. In other regions, Europe, boreal Asia, Africa, South
87 Asia, and Oceania, it was difficult to determine whether those regions act as a net sink or source because
88 of the large spread in estimates from atmospheric inversions. These results highlight two research
89 directions to improve the robustness of CO₂ budgets: (1) to increase representation of processes in
90 biosphere models that could contribute to fill the budget gaps, such as forest regrowth and forest
91 degradation, and (2) to reduce sink-source compensation between regions (dipoles) in atmospheric
92 inversion so that their estimates become more comparable. Advancements on both research areas will
93 increase the level of agreement between the top-down and bottom-up approaches and yield more robust
94 knowledge of regional CO₂ budgets.

95
96 **Keywords:** terrestrial CO₂ budget, net CO₂ flux, atmospheric inversion, biosphere model, carbon stock
97 change, residual land uptake, land-use change emissions, riverine carbon export, CO₂ evasion

98 **1. INTRODUCTION**

99 Understanding the mitigation potential of the terrestrial biosphere against anthropogenic CO₂
100 emissions hinges upon accurate assessment of the net atmosphere-land CO₂ flux (net CO₂ flux, - for a
101 net sink and + for a net source). Our ability to diagnose CO₂ sink-source patterns of the net CO₂ flux has
102 progressed owing to the development of “top-down” atmospheric inversions (Peylin et al., 2013;
103 Thompson et al., 2016) and “bottom-up” biosphere models (Sitch et al., 2008, 2015). Compared with
104 early studies that varied by more than 3.0 Pg C yr⁻¹ in their estimates of northern and tropical CO₂ fluxes
105 (e.g., Gurney et al., 2002; Jacobson, Fletcher, Gruber, Sarmiento, & Gloor, 2007; Peylin, Baker,
106 Sarmiento, Ciais, & Bousquet, 2002; Rödenbeck, Houweling, Gloor, & Heimann, 2003), net CO₂ fluxes
107 by current atmospheric inversions are converging around a sink of 1.0 to 2.0 Pg C yr⁻¹ in northern
108 extratropical (NE) lands and a small net flux in southern–tropical (ST) lands, due to improvements in
109 the transport processes modeling and abundance of aircraft and vessel observations, along with
110 improved in situ CO₂ observation networks (Gaubert et al., 2019; Stephens et al., 2007). Likewise, net
111 CO₂ fluxes simulated by biosphere models have become roughly consistent with this pattern, especially
112 in ST lands, due to the offset of land-use change (LUC) emissions with enhanced CO₂ uptake by the
113 stimulating effect of rising atmospheric CO₂ on plant photosynthesis (Schimel, Stephens, & Fisher,
114 2015). However, disagreements in the CO₂ budgets between top-down and bottom-up approaches
115 remain nontrivial at regional scales (Cervarich et al., 2016; Ciais et al., 2013; Kondo, Ichii, Takagi, &
116 Sasakawa, 2015). In the fifth assessment report of Intergovernmental Panel on Climate Change (IPCC
117 AR5), the sign and magnitude of regional CO₂ budget estimates were still contradictory between
118 atmospheric inversions and biosphere models for some regions (Ciais et al., 2013).

119 These previous syntheses highlight the challenges of reconciling the top-down and bottom-up
120 approaches and the importance of spatial scale in evaluating agreement and uncertainties. When
121 comparing CO₂ budgets of multiple methods, understanding the definition of the net CO₂ flux and
122 associated component fluxes that are included in developing the CO₂ budgets become increasingly
123 important because these could lead to either a “total” or “partial” exchange of CO₂ between the
124 atmosphere and land depending upon the methods employed. The former applies to methods that use
125 atmospheric CO₂ concentrations as a basis for estimation such as atmospheric inversions (Peylin et al.,
126 2013). The latter applies to methods that account for known processes in the carbon cycle interacting
127 with the biosphere such as biosphere models (Sitch et al., 2015). Major terms that cause challenges in
128 comparing atmospheric inversions and biosphere models at the time of the IPCC AR5 can be: (1)

129 hydrosphere fluxes, such as lateral riverine carbon export and CO₂ evasion from rivers and lakes,
130 included in atmospheric inversions, but not simulated in biosphere models, and (2) the incomplete
131 representation of CO₂ fluxes from land-use and management in biosphere models. Mitigating these
132 differences in terminology will advance our understanding of net CO₂ flux at regional scales which so
133 far has remained unresolved.

134 To address the current state of our knowledge on terrestrial CO₂ budgets and the level of
135 reconciliation between current modeling methods, CO₂ budget assessments at global, hemispheric, and
136 regional scales need to be reanalyzed with consistent datasets and definitions of the component fluxes
137 that determine net CO₂ flux. Based on the net CO₂ flux defined as “the atmosphere-biosphere CO₂
138 exchange” (excluding hydrosphere fluxes), we investigate net CO₂ fluxes estimated for the decade of
139 2000s (2000–2009) using fluxes adjusted around a consistent definition of the CO₂ exchange. These are
140 compared with reproduced results of the IPCC AR5 obtained using inconsistent definitions, to determine
141 how definitions play a role in reconciliation between the modeling methods. Aimed at serving as a
142 useful reference, this study provides a thorough comparison between atmospheric inversions and
143 biosphere models, and also among other existing estimates of global and regional CO₂ budgets based on
144 forest inventories, remote sensing, atmospheric O₂ measurements, the residuals from non-terrestrial
145 components of global CO₂ budgets, and previous regional budget assessments from the REgional
146 Carbon Cycle Assessment and Processes (RECCAP, Canadell et al., 2011). Through these comparisons,
147 we highlight potential difficulties faced by current CO₂ budget assessments, and suggests ways forward
148 to increase the level of agreement between top-down and bottom-up approaches yielding more robust
149 knowledge of CO₂ budgets.

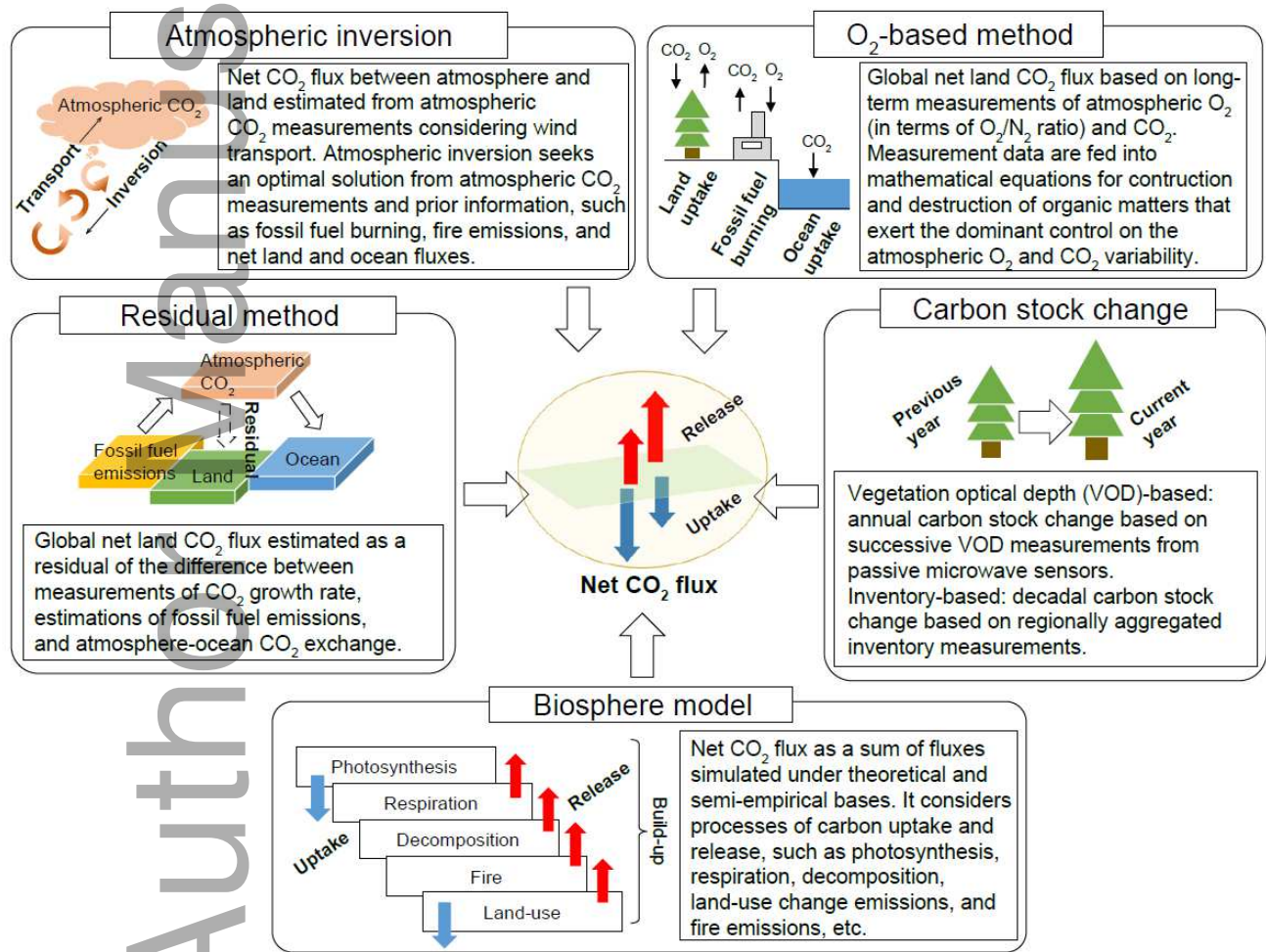
150

151 **2. MATERIALS AND METHODS**

152 **2.1 Definition of net CO₂ flux**

153 We define the net CO₂ flux as the “atmosphere-biosphere CO₂ exchange”, comprising components
154 such as photosynthesis, autotrophic and heterotrophic respirations, fire emissions, and CO₂ fluxes
155 associated with land-use and land-cover changes. Adjustments based on the proposed definition of net
156 CO₂ flux were applied to the methods described herein where relevant (Fig. 1; Spatial and temporal
157 applicability of the methods is shown in Table S1). Biosphere models comply with this definition, as
158 they consider numerous processes of atmosphere-land biogeochemistry, including LUC fluxes in the
159 latest development (Le Quéré et al. 2018a). A method based on carbon stock changes from the

160 compilation of forest inventories (ΔC_{IM} , Pan et al., 2011) also complies with this definition. The
 161 Vegetation Optical Depth (VOD) derived from passive microwave sensors (e.g., Liu et al., 2015) is only
 162 applicable to aboveground vegetation, but can be supplemented by inventories of missing belowground
 163 components to represent the total stock change (ΔC_{VOD}). Methods that consider interactions beyond
 164 those with the biosphere, such as atmospheric inversions, and global land uptake assessments based on a
 165 residual of non-terrestrial components of global CO₂ budgets (residual method, Le Quéré et al., 2018a)
 166 and based on decadal O₂ and CO₂ trends in the atmosphere (O₂-based method, Keeling & Manning,
 167 2014) can roughly comply with the proposed definition when the hydrosphere fluxes are excluded from
 168 their budget estimates, as we discuss further in this paper.



169
 170 **FIGURE 1.** Methods of terrestrial net CO₂ flux estimation.

171
 172 **2.2 Independent methods of estimating net CO₂ flux**

174 **2.2.1 Atmospheric inversions**

175 The net CO₂ flux from atmospheric inversions was represented by eight inversions (Table 1). These
176 inversions estimate net CO₂ flux through the assimilation of continuous or discrete atmospheric CO₂
177 measurements from global networks (e.g., World Data Centre for Greenhouse Gases, WDCGG; and the
178 observation package (ObsPack) from the NOAA Earth System Research Laboratory, NOAA/ESRL) in
179 transport model, with prior information (e.g., net land flux, net ocean flux, fire emissions, and fossil fuel
180 emissions). The choices of CO₂ measurements and prior fluxes differ for each inversion system, as well
181 as the spatial resolution and period of inverted fluxes (Table 1).

182 For each inversion, posterior land flux was adjusted by the difference between the respective fossil
183 fuel emissions prescribed in the inversion and a reference emission estimate. This “fossil fuel
184 adjustment” is a necessary procedure for reducing variability in posterior fluxes, as differences in
185 prescribed fossil fuel emissions largely affect posterior fluxes (Peylin et al., 2013), especially for recent
186 periods for which the uncertainty in fossil fuel emissions remains large (Ballantyne et al., 2015). We
187 applied the fossil fuel adjustment using the emission dataset prescribed in ACTM (Table 1), showing a
188 central tendency of global interannual variability among inversions, as the reference emission.

Author Manuscript

189 **TABLE 1.** Configuration of the atmospheric CO₂ inversion systems used in this study.

Inversion system (in-text abbreviation)	No. of region	Time period	IAV prior [#]	No. of observations	Transport model	Meteorology	Prior fluxes				Reference
							Land	Ocean	Biomass Burning	Fossil fuel emissions	
ACTM (ACTM)	84	1990–2011	Yes: FF, LA No: SA	73 (GLOBALVIEW)	JAMSTEC's Atmospheric Chemistry-Transport Model (ACTM)	NCEP	Three-hourly flux from CASA	Monthly flux from the LDEO (Takahashi) Surface pCO ₂ database	--	EDGAR v4.2 rescaled global total to CDIAC	Saeki & Patra (2017)
MIROC4-ACTM (MACTM)	84	1996–2015	Yes: FF, LA No: SA	42 sites (NOAA ESRL ObsPack & JMA)	Updated ACTM with MIROC4-ESM	JRA-55	Three-hourly flux from CASA	Monthly flux from the LDEO	--	EDGAR v4.3.2	Patra et al. (2018); Le Quéré et al. (2018b)
CAMS v18r1 (CAMS)	Grid cells (3.75° × 2.5°)	1979-2015	Yes: FF No: BB, LA, SA	81 (NOAA ESRL ObsPack)	Tracer Transport Model version 5 (TM5)	ECMWF	Three-hourly flux from ORCHIDEE	Monthly flux from the LDEO (Takahashi) Surface pCO ₂ database	GFAS	EDGAR v4.2 rescaled global total to CDIAC	Chevallier et al. (2010)
CCAM (CCAM)	94 land, 52 ocean	1993-2012	Yes: FF No: LA, SA	69 (GLOBALVIEW)	CSIRO Conformal-cubic Atmospheric Model (CCAM)	NCEP	Monthly flux from CASA	Monthly flux from the LDEO (Takahashi) Surface pCO ₂ database	--	EDGAR v4.2 rescaled regionally to CDIAC	McGregor & Dix (2008)
Carbon Tracker2017 (CT2017)	Grid cells (1.0° × 1.0°)	2000-2016	Yes: FF, BB, LA, SA	254 (from 55 institutions)	Tracer Transport Model version 5 (TM5)	ECMWF and ERA	Monthly CASA flux downscaled to 90-minute flux	Ocean inversion fluxes and monthly flux from the LDEO Surface pCO ₂ database	GFED4.1s and GFED_CM S	ODIAC2016 and Miller emissions datasets	Peters et al. (2007)
GELCA_CAO (GELCA CAO)	Grid cells (1.0° × 1.0°)	2000-2013	Yes: FF, BB, LA, SA	NOAA ESRL ObsPack	Coupled GELCA-NIES 08.1 Eulerian model	JCDAS	Daily flux from VISIT	Monthly flux from 4D-var + OTTM based on	GFED	ODIAC	Zhuravlev, Khattatov, & Kiryushov, &

								<i>p</i> CO ₂ data			Maksyutov (2011)
JENA s93_v4.2 (JENA s93)	Grid-cells (about 4.0° × 5.0°)	1993-2016	Yes: FF No: LA, SA	35 (from various institutions)	Tracer Transport Model version 3 (TM3)	NCEP	Zero values	Monthly climatological flux based on an interpolation of <i>p</i> CO ₂ data	--	Monthly values from CDIAC	Rödenbeck, Zaehle, Keeling, & Heimann (2018)
JMA2018 (JMA)	22	1985–2016	Yes: FF, SA No: LA	88 (WDCGG) 16 (aircraft observations), 59 (vessel observations)	JMA atmospheric transport model (based upon JMA global weather forecasting model)	JRA-55	Monthly flux from CASA	Monthly flux from the JMA (Iida et al., 2015)	--	CDIAC2016 rescaled global total to Global Carbon Budget (2017v1.2)	Update of Maki et al. (2010)

190 #Abbreviations: biomass burning emission (BB), fossil fuel emission (FF), land-air CO₂ exchange (LA), and sea-air CO₂ exchange (SA).

191

192 **2.2.2 Biosphere models**

193 Simulations from TRENDY v6 (Le Quéré et al., 2018a) represent the net CO₂ flux from the
194 biosphere models of this study (Table 2). These simulations were prepared with a consistent forcing
195 dataset: a global atmospheric CO₂ concentrations for 1860–2016 based on ice core measurements and
196 stationary observations from NOAA, a gridded climate dataset (CRU-NCEP v8) for 1901–2016 (Viovy,
197 2018), and a gridded annual land-use and land-cover change dataset for 1860–2016 (Hurtt et al., 2017;
198 Klein Goldewijk, Beusen, Doelman, & Stehfest, 2017). The TRENDY models carried out three types of
199 simulations: S1 that used varied atmospheric CO₂, fixed climate (1901–1920) and fixed land-use and
200 land-cover (1860), S2 that used varied CO₂ and climate (with fixed land-use and land-cover at 1860),
201 and S3 that varied all three drivers. For each simulation, the models first established an equilibrium
202 carbon balance by a spin-up run, forced with the 1860 CO₂ concentration (287.14 ppm), recycling
203 climate variability from 1901–1920, and constant 1860 crop and pasture distributions.

204 Attributes of the net CO₂ flux (i.e. the effects of CO₂, climate, and LUC) were extracted by
205 separating flux signals in the S1, S2, and S3 simulations (Friedlingstein et al., 2006). The net CO₂ flux
206 of S3 represented the estimate most closely matching observations, including the interactions between
207 CO₂, climate, and LUC effects on the ecosystem carbon cycling. Those from S1 and S2 represented
208 partial contributions to the net CO₂ flux, isolating the CO₂ effect and CO₂+climate effects on the net
209 CO₂ flux, respectively. The LUC effect on the net CO₂ flux was extracted by subtracting estimates of S2
210 from that of S3. Similarly, the effect of climate was extracted by subtracting the net CO₂ flux of S1 from
211 that of S2.

212 **TABLE 2.** Configuration of the TRENDY models used in this study.

Biosphere model	Spatial resolution	Carbon-Nitrogen coupling	Fire simulation (including peat fire)	Age class	Land use change scheme					Reference
					Distinction between primary and secondary lands	Wood harvest	Shifting cultivation	Crop harvest (crop species: C, managed grassland :G)	Degradation	
CABLE	0.5° × 0.5°	Yes	No	Yes	Yes	Yes	Yes	Yes: G	No	Haverd et al. (2018)
CLM	1.9° × 2.5°	Yes	Yes (Yes)	No	Yes	Yes	Yes	Yes: G	No	Oleson et al. (2013)
DLEM	0.5° × 0.5°	Yes	No	No	Yes	Yes	No	Yes: G	No	Tian et al. (2015)
ISAM	0.5° × 0.5°	Yes	No	No	Yes	Yes	No	Yes: G	No	Jain, Meiyappan, Song, & House (2013)
LPJ-GUESS	0.5° × 0.5°	Yes	Yes (No)	No	Yes	Yes	Yes	Yes: C	No	Smith et al. (2014)
LPJ-wsl	0.5° × 0.5°	No	Yes (No)	No	Yes	No	No	Yes: G	No	Sitch et al. (2003)
LPX-Bern	1.0° × 1.0°	Yes	Yes (No)	No	No	No	No	Yes: G	No	Keller et al. (2017)
ORCHIDEE	0.5° × 0.5°	No	No	No	Yes	Yes	No	Yes: G	No	Krinner et al. (2005)
ORCHIDEE-MICT	1.0° × 1.0°	No	Yes (No)	No	Yes	No	No	Yes: C	No	Guimberteau et al. (2018)
VISIT	0.5° × 0.5°	No	Yes (No)	No	Yes	Yes	Yes	Yes: G	No	Kato, Kinoshita, Ito, Kawamiya, & Yamagata (2013)

214

215 **2.2.3 Carbon stock changes, O₂-based method, residual method, and RECCAP**

216 Inventory-based carbon stock changes (ΔC_{IM}) were estimated by incorporating information on forest
217 area and biomass density obtained from (i) United Nations Global Forest Resources Assessment reports
218 (Food and Agriculture Organization, 2006, 2010), (ii) deforestation and afforestation estimates from a
219 book-keeping model (Houghton, 2007), and (iii) the observed carbon pools for regions around the
220 globe. From these datasets, the sums of carbon stocks for intact and regrowth forests and soil carbon for
221 2000 and 2007 were used to calculate regional carbon stock changes (Pan et al., 2011), except for South
222 Asia where a missing estimate was supplemented by inventory and forest area data for 1992–2002 from
223 Kaula, Dadhwal, and Mohren (2009). To estimate VOD-based carbon stock change (ΔC_{VOD}) for the
224 2000s, we used the satellite-derived gridded aboveground biomass from Global Aboveground Biomass
225 Carbon v1.0 (Liu et al., 2015). The VOD-based aboveground biomass is estimated based on an
226 empirical relationship between the gridded aboveground biomass for tropical regions (Saatchi et al.,
227 2011) and harmonized passive microwave observations. VOD only measures aboveground backscatter,
228 therefore belowground biomass was estimated as a constant fraction of the estimated aboveground
229 biomass (Liu et al., 2015). To provide more reliable estimates, we replaced this belowground biomass of
230 ΔC_{VOD} with the data used for ΔC_{IM} .

231 The O₂-based method provides a mean annual global CO₂ budget for the land and ocean based on
232 destructive and constructive O₂ and CO₂ processes (Keeling & Manning, 2014). This approach utilizes
233 long-term measurements of CO₂ and the O₂/N₂ molar ratio between a sample and a reference, expressed
234 as $\delta(O_2/N_2)$, as changes in the global mean molar fraction of CO₂ and $\delta(O_2/N_2)$ are related to the net
235 sources and sinks of CO₂, O₂, and N₂ in the atmosphere. The budget used in this study was estimated for
236 2000–2010 by Keeling and Manning (2014). The residual method from the Global Carbon Project (Le
237 Quéré et al., 2018a) provided the global annual budget of land CO₂ uptake calculated as the difference
238 between the other terms in the global carbon budget, i.e., fossil fuel emissions minus the CO₂ growth
239 rate and the net ocean uptake simulated by biogeochemical models. The budget of this method for the
240 2000s was calculated using the data of Le Quéré et al. (2018a). The RECCAP project quantified regional
241 anthropogenic and biogenic CO₂ budgets by integrating CO₂ fluxes from multiple independent
242 approaches, including biosphere models, atmospheric inversions, and inventories (Canadell et al., 2011).
243 Based on the available major and minor fluxes and through consideration of the reliability of each of the

244 fluxes, the regional CO₂ budget was estimated for global regions. The regional budgets used in this
245 study were from re-calculated estimates based on the RECCAP studies in Li et al. (2016).

246

247 **2.3 Adjustments for the atmosphere-biosphere CO₂ exchange estimation**

248 To yield the atmosphere-biosphere CO₂ exchange, global gridded data of lateral riverine carbon
249 export and CO₂ evasion from rivers and lakes were used to remove the hydrosphere components from
250 the fossil fuel adjusted CO₂ budgets of the atmospheric inversions. Global lateral riverine carbon
251 including dissolved organic and inorganic carbon (DOC and DIC, respectively) was obtained from the
252 multi-form model of nutrient exports by NEWS 2 (Mayorga et al. 2010). Global river CO₂ evasion was
253 derived from the empirical river water *p*CO₂ model and global maps of stream surface area and gas
254 exchange velocities (Lauerwald, Laruelle, Hartmann, Ciais, & Regnier, 2015). Global lake CO₂ evasion
255 was estimated based on lake *p*CO₂, total lake/reservoir surface area, and total CO₂ evasions for 231
256 coastal regions (Raymond et al., 2013), subsequently downscaled to a continuous grid scale via the
257 Global Lakes and Wetland Database (Zscheischler et al., 2017).

258 These data were also used to derive the atmosphere-biosphere CO₂ exchange for the O₂-based
259 method and RECCAP. The O₂-based method and RECCAP account for lateral riverine exports as a part
260 of the land biosphere flux. Thus, we excluded annual riverine DOC and DIC fluxes from the global
261 budget estimates of both methods using the data described above. Global CO₂ uptake by the residual
262 method includes only riverine carbon exports due to anthropogenic perturbations (Le Quéré et al.,
263 2018b). To remove that flux from the residual method, an estimate of the anthropogenic component of
264 river flux from Regnier et al. (2018) was used.

265

266 **2.4 A constraint for the global budget**

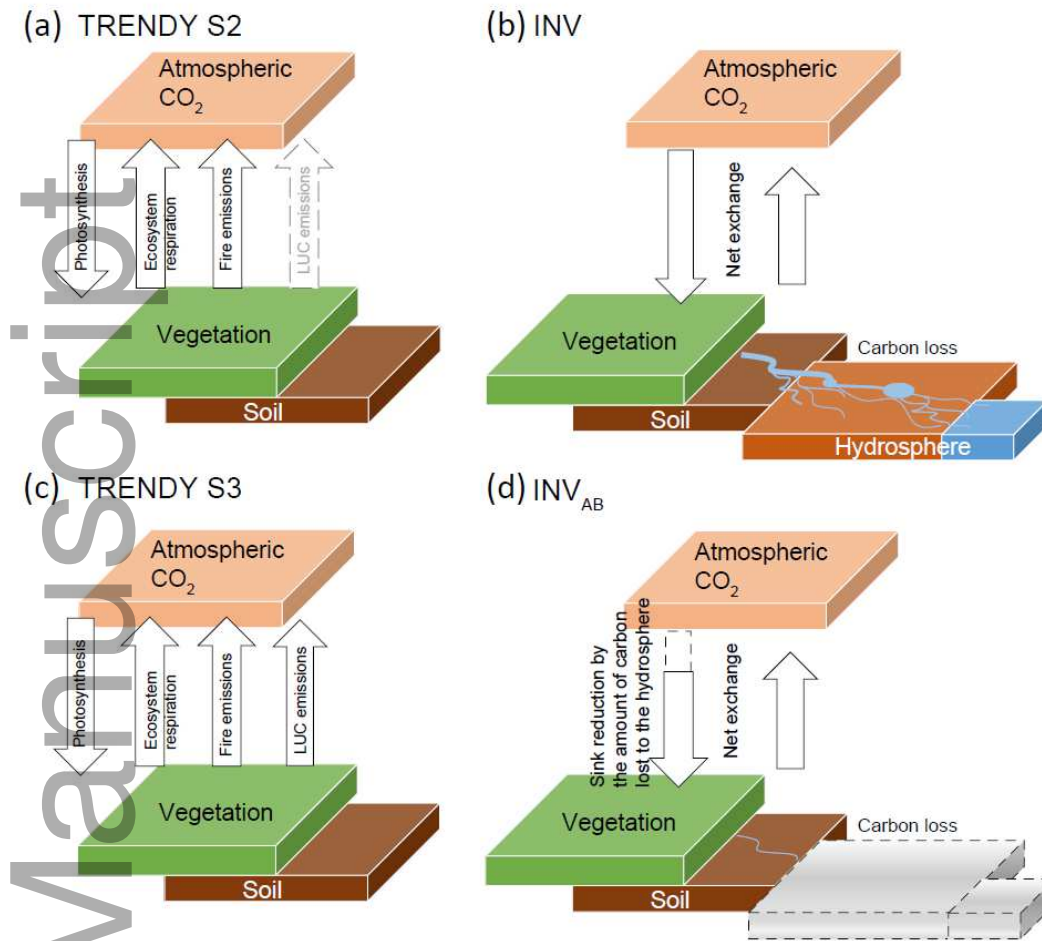
267 Owing to atmospheric observations, the CO₂ budget at the global scale is the best understood among
268 those at other scales (Le Quéré et al., 2018a). To analyze CO₂ budgets at multiple scales, it is important
269 to have consistent global CO₂ budgets so that results of hemispheric and regional budgets would not be
270 misinterpreted due to outliers of global budget estimates. Therefore, we defined a criterion, based on the
271 global CO₂ budget from the residual method and ±1.0 Pg C yr⁻¹ uncertainties, to constrain global CO₂
272 budgets from the top-down and bottom-up models for the 2000s. All eight atmospheric inversions of this
273 study satisfied this criterion, since the atmospheric CO₂ growth rate was used to constraint atmospheric

274 inversions. As for biosphere models, among the TRENDY models that provided net CO₂ fluxes of all
275 three experiments, ten models satisfied this criterion (Table 2).

276

277 3. GLOBAL AND HEMISPHERIC BUDGETS

278 To articulate differences from results of the IPCC AR5, we compared experiments from TRENDY
279 (S2: not including time-varying LUC simulation, and S3: including time-varying LUC simulation), and
280 atmospheric inversions before (INV) and after correcting for the hydrosphere components (INV_{AB}
281 denotes inversions adjusted for the atmosphere-biosphere CO₂ exchange). TRENDY S3 and INV_{AB}
282 represented “best estimates” of the net CO₂ flux, and TRENDY S2 and INV represented estimates
283 reproduced using the IPCC AR5 configuration (Fig. 2). As illustrated in Figure 3a, global CO₂ budgets
284 by TRENDY S2 (-2.6 [-2.9, -2.1] Pg C yr⁻¹: medians [lower, upper quartiles]) and INV (-2.3 [-2.5, -1.7]
285 Pg C yr⁻¹) largely overestimated the amount of CO₂ uptake compared with other independent estimates:
286 ΔC_{VOID} (-1.2 Pg C yr⁻¹), ΔC_{IM} (-1.2 Pg C yr⁻¹), the residual method (-0.9 Pg C yr⁻¹), O₂-based method (-
287 0.7 Pg C yr⁻¹), and RECCAP (-1.3±0.6 Pg C yr⁻¹, mean±1σ). This overestimated CO₂ uptake is likely a
288 consequence of missing and excess components needed to satisfy the net CO₂ flux definition.
289 Meanwhile, upward shifts in the net CO₂ flux caused by accounting for LUC emissions in the biosphere
290 models and discounting the hydrosphere fluxes in the atmospheric inversions led to a close agreement in
291 global CO₂ budgets with respect to the other independent estimates and with each other, where
292 TRENDY S3 estimated -0.9 [-1.4, -0.8] Pg C yr⁻¹ and INV_{AB} estimated -0.9 [-1.2, -0.4] Pg C yr⁻¹ (Fig.
293 3a; interannual variability (IAV) shown in Fig. S1).



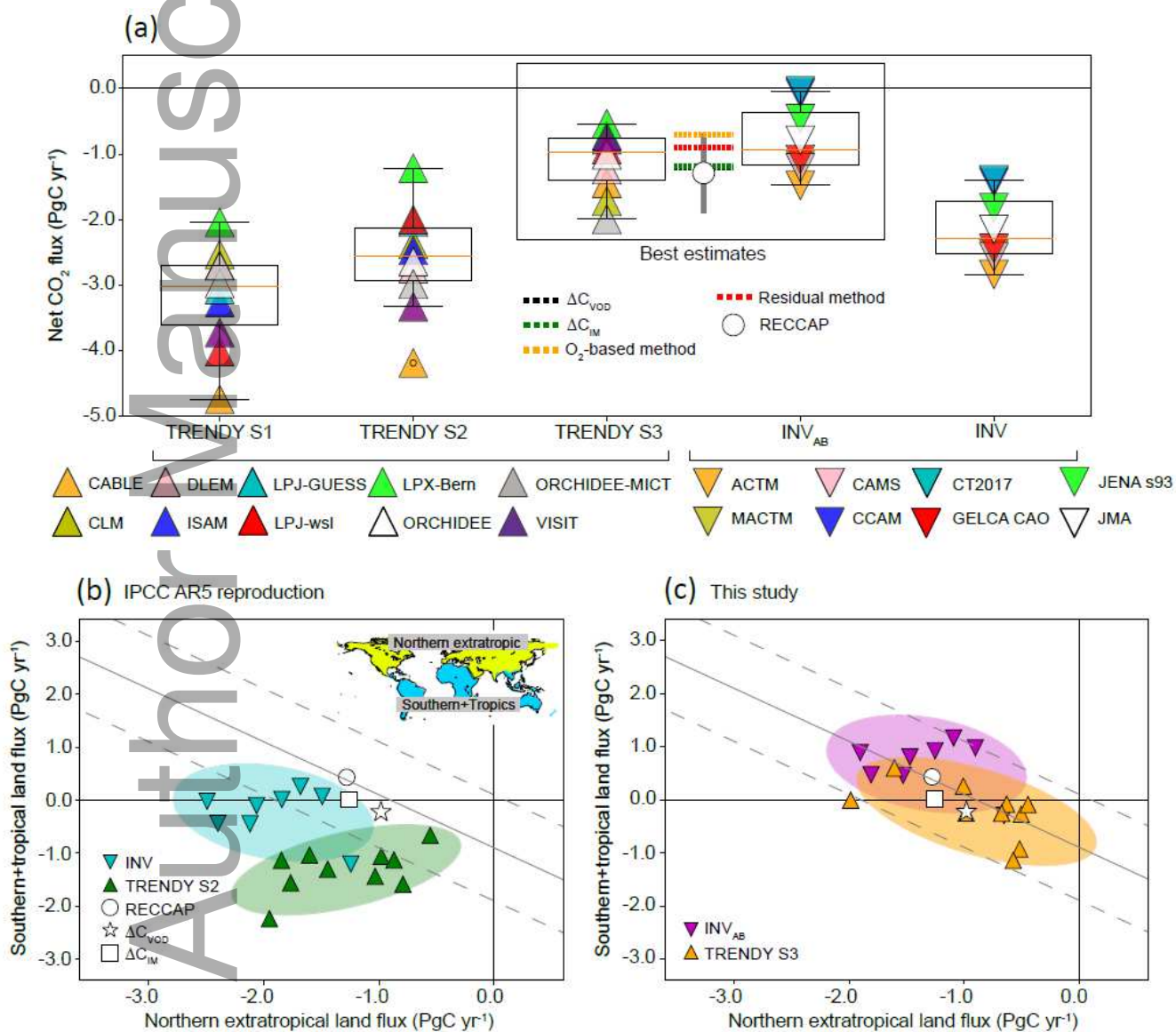
294

295 **FIGURE 2.** Differences in definition of the net CO₂ flux. Schematics show the components of the net CO₂ flux
 296 considered in: **a)** TRENDY S2 (biosphere models without LUC), **b)** INV (atmospheric inversions including
 297 hydrospheric components), **c)** TRENDY S3 (biosphere models including LUC), and **d)** INV_{AB} (atmospheric
 298 inversions excluding hydrospheric components).

299

300 The global CO₂ budget largely consists of fluxes from northern boreal-temperate and pantropical
 301 ecosystems, with the former accounting for a large part of the global sink and the latter for a large part
 302 of the global LUC emissions (Ciais et al., 2019; Le Quéré et al., 2018b). That is, the well-constrained
 303 global CO₂ budgets among the methods should accompany a consistent budget partitioning between
 304 those regions. To evaluate this aspect, we applied the so-called “diver down” plot of Schimel, Stephens,
 305 and Fisher (2015) to better understand global CO₂ budget partitioning into NE and ST lands (Fig. 3b, c).
 306 The reproduced IPCC AR5 results (TRENDY S2 and INV) exhibited limited overlap with each other
 307 (Fig. 3b). INV produced relatively strong sinks of -1.2 to -2.5 Pg C yr⁻¹ in NE and a small net flux in ST

308 lands. With the absence of LUC emissions, TRENDY S2 resulted in a net sink for both NE and ST lands,
 309 spanning approximately -1.0 to -2.0 Pg C yr^{-1} . Including simulated LUC fluxes in biosphere models and
 310 removing the hydrosphere fluxes from atmospheric inversions shifted the NE and ST land fluxes of the
 311 two methods towards a reduced sink or net source, leading to an overlap between TRENDY S3 and
 312 INV_{AB} (Fig. 3c; IAV shown in Fig. S2) and with $\Delta\text{C}_{\text{VOD}}$, $\Delta\text{C}_{\text{IM}}$, and RECCAP (Fig. 3c). However,
 313 agreements between TRENDY S3 and INV_{AB} are not yet robust, as the distribution of INV_{AB} leans more
 314 towards a net sink in NE lands (-2.2 to -0.7 Pg C yr^{-1}) and a net source in ST lands (-0.4 to 1.0 Pg C yr^{-1})
 315 than that of TRENDY S3: -2.0 to -0.5 Pg C yr^{-1} in NE and -1.1 to 0.6 Pg C yr^{-1} in ST lands.

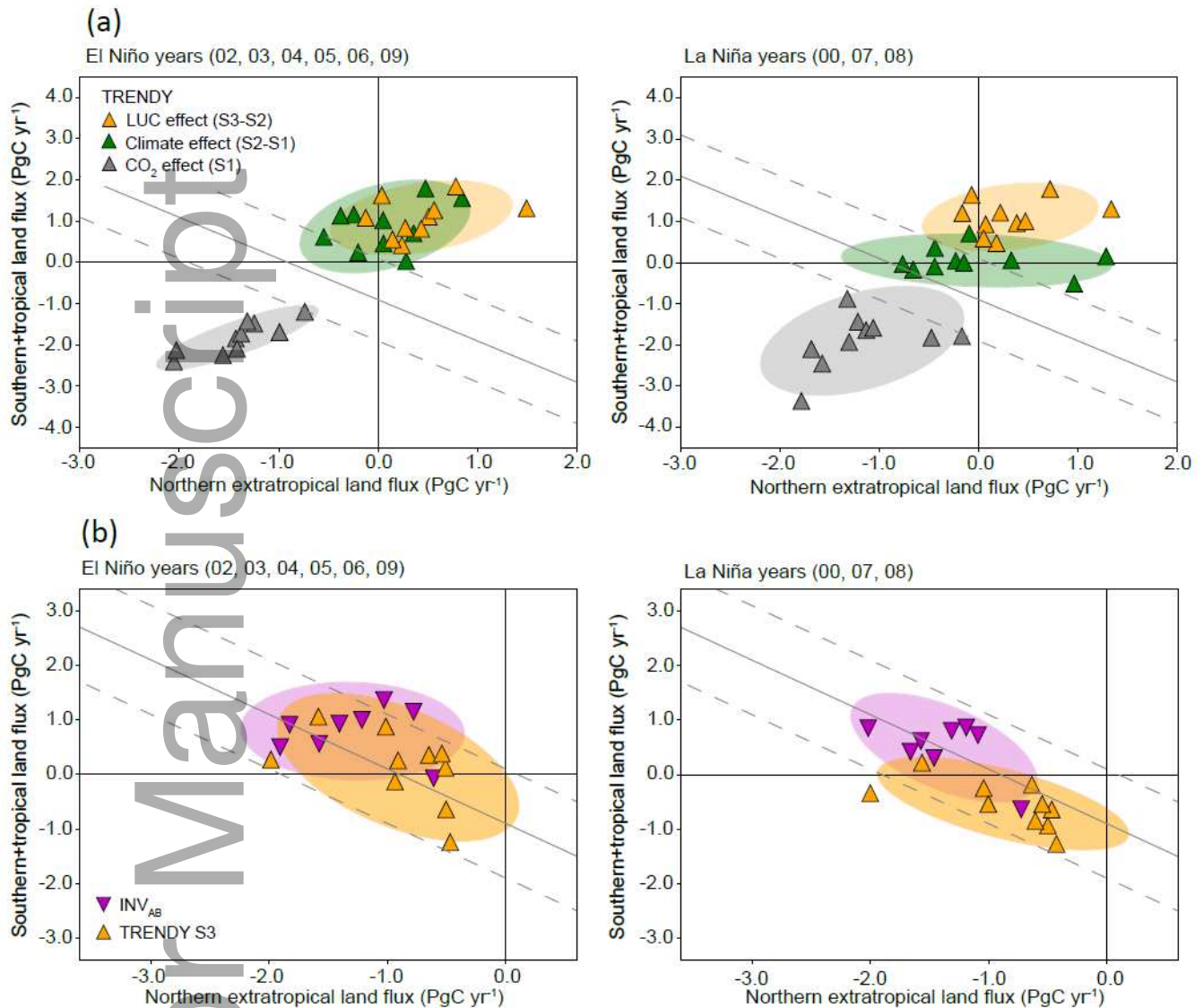


316
 317 **FIGURE 3.** Improved agreement of global and hemispheric net CO₂ flux estimates over the IPCC AR5. **a)** Global
 318 CO₂ budgets for the 2000s from the biosphere models (upper triangles), atmospheric inversions (lower triangles),

319 carbon stock changes: ΔC_{VOD} (black dashed line) and ΔC_{IM} (green dashed line), O₂-based method (yellow dashed
320 line), residual method (red dashed line), and estimates from the RECCAP project (circle representing the mean
321 value and bar representing the 1 σ uncertainty). Box plots are shown for the biosphere models (three TRENDY
322 simulations, S1, S2, and S3) and atmospheric inversions (INV and INV_{AB}). Partitioning of the global CO₂ budget
323 into northern extratropical (NE) and southern-tropical (ST) lands (diver-down plot) for **b**) TRENDY S2 and INV
324 (IPCC AR5 reproduction), and **c**) TRENDY S3 and INV_{AB} (results from this study). Gray lines are the constraint
325 on global CO₂ budgets represented by the global budget estimate from the residual method, with ± 1.0 Pg C yr⁻¹
326 uncertainty. Results that fall within the constraints are combinations of NE and ST land budgets that preserve the
327 reference value of global CO₂ budget. Individual model estimates and error ellipse of 2 σ range are shown for
328 TRENDY S2 and S3 (green and orange upper triangles, respectively), and INV and INV_{AB} (cyan and purple lower
329 triangles, respectively), along with the independent estimates from carbon stock changes: ΔC_{VOD} and ΔC_{IM} (star
330 and square, respectively) and estimate from the RECCAP project (circle representing the mean value).

331

332 Figure 3c illustrates the results only of the net balance of CO₂ fluxes. To gain confidence in the
333 overlapping pattern between the two methods, it is necessary to understand changes in the patterns of
334 sinks and sources induced by the major processes governing the net CO₂ flux. The effect of increasing
335 CO₂ concentration on photosynthesis (the CO₂ effect) is considered the dominant driver of current
336 terrestrial CO₂ uptake (Keenan et al., 2016; Keenan & Williams, 2018; Kondo et al., 2018a; Schimel,
337 Stephens, & Fisher, 2015), and LUC activities (the LUC effect) are the major net emissions source from
338 ecosystems to the atmosphere (Arneeth et al., 2017; Kondo et al., 2018b). The net CO₂ flux of TRENDY
339 S3 decomposed into three attributes confirms that the CO₂ and LUC effects are the major sink and
340 source components in NE and ST lands, respectively (Fig. 4a). However, the climate effect should not
341 be overlooked, as it induces substantial changes in sink-source patterns during El Niño and La Niña
342 phases, especially in ST lands (Fig. 4a). Importantly, the overlap between TRENDY S3 and INV_{AB}
343 holds not only for the decadal mean (Fig. 3c), but also for the El Niño and La Niña phases during the
344 2000s (Fig. 4b; IAV and seasonality of ST land fluxes shown in Fig. S3), indicating that large-scale flux
345 changes in response to El Niño-Southern Oscillation (ENSO) are similar in the atmospheric inversions
346 and biosphere models.



347

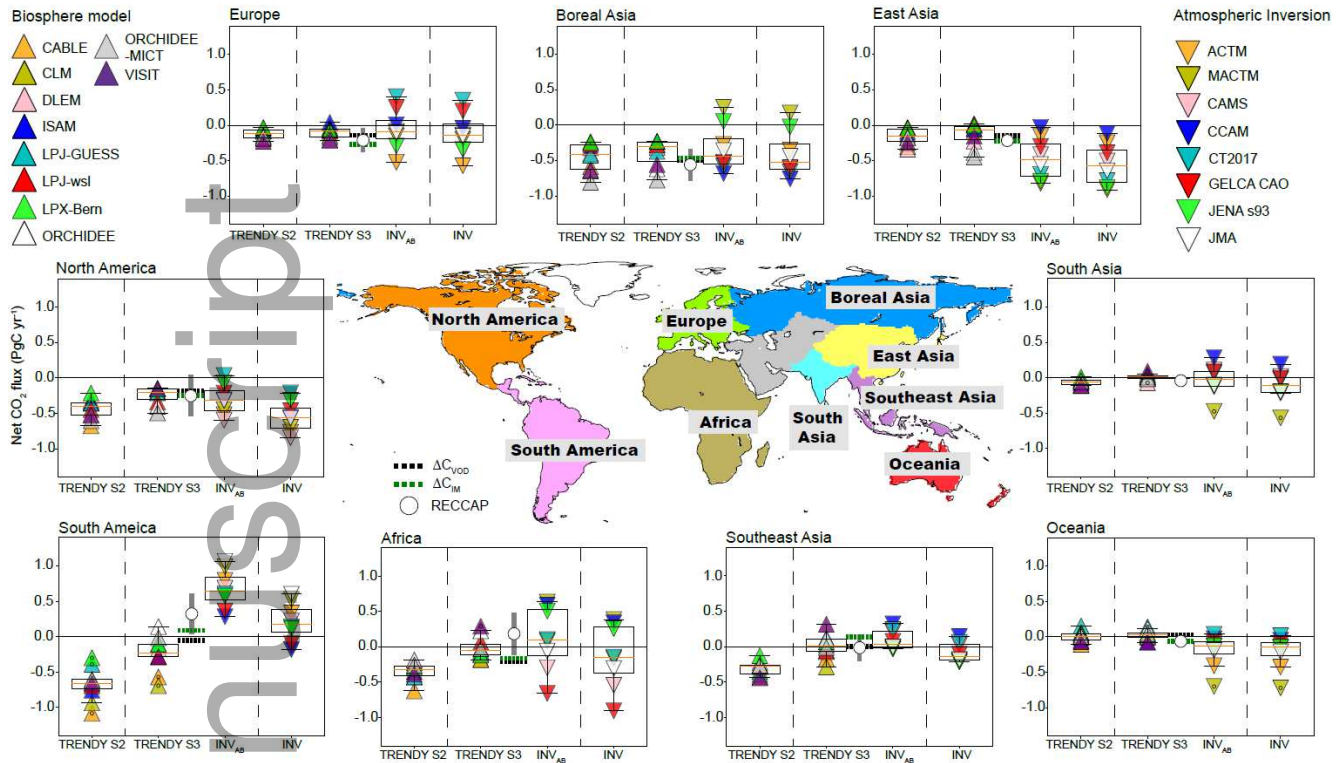
348 **FIGURE 4.** Patterns of global CO₂ budget partitioned into hemispheres under ENSO variability. Partitioning of
 349 global CO₂ budget into NE and ST lands (diver-down plots), during El Niño years (2002, 03, 04, 05, 06, and 09)
 350 and La Niña years (2000, 07, and 08) are shown for: **a)** each attribute of the net CO₂ flux by TRENDY S3, CO₂
 351 effect (TRENDY S1: grey upper triangles), climate effect (TRENDY S2-S1: green upper triangles), and LUC
 352 effect (TRENDY S3-S2: orange upper triangles) and **b)** the net CO₂ fluxes of INV_{AB} and TRENDY S3. El Niño
 353 years are the years that have six-month averaged Multivariate ENSO Index (MEI) values >0.5 within a year, and
 354 La Niña years are the years that have MEI values <-0.5 within a year. Gray lines represent the global budget
 355 constraint and ±1.0 Pg C yr⁻¹ uncertainty same as in Figure 3c.

356

357 4. REGIONAL BUDGETS

358 We further partitioned hemispheric budgets into nine regions. Regional CO₂ budgets were overall
359 comparable between TRENDY S3 and INV_{AB}, but the degree of agreement differed by region (Fig. 5;
360 IAV shown in Fig. S4). Among the nine regions, the ranges of budget estimates were proximate among
361 INV_{AB}, TRENDY S3, and the other independent estimates for North America and Southeast Asia. A
362 notable improvement was identified in Southeast Asia, where reduced CO₂ sinks by accounting for LUC
363 fluxes in biosphere models and discounting for the hydrosphere fluxes from atmospheric inversions
364 resulted in close agreement between INV_{AB} (0.01 [-0.04, 0.20] Pg C yr⁻¹) and TRENDY S3 (-0.01 [-0.06,
365 0.10] Pg C yr⁻¹). Budget estimates for Europe, boreal Asia, Africa, South Asia, and Oceania overlapped,
366 but with a larger range in INV_{AB} than in TRENDY S3 (Fig. 5). In Africa, adjustments for the missing
367 and excess fluxes in the two modeling methods seemingly mitigated the gap between median INV and
368 TRENDY S2 values; however, a range > 1.0 Pg C yr⁻¹ in the individual estimates of INV_{AB} rendered
369 comparison with TRENDY S3 difficult.

370 Budget estimates for East Asia and South America showed notable differences between INV_{AB} and
371 TRENDY S3 (Fig. 5). In East Asia, the budget estimates by both INV_{AB} and TRENDY S3 indicated a
372 net sink, but INV_{AB} (-0.5 [-0.7, -0.3] Pg C yr⁻¹) leaned towards a greater net sink than TRENDY S3 (-
373 0.07 [-0.20, -0.01] Pg C yr⁻¹). In South America, INV_{AB} leaned towards a net source contrary to the net
374 sink indicated by TRENDY S3. The gap in South America was the most notable, with budget estimates
375 barely overlapping between INV_{AB} (0.6 [0.5, 0.8] Pg C yr⁻¹) and TRENDY S3 (-0.2 [-0.3, -0.1] Pg C yr⁻¹).
376 In this region, the flux adjustments did not reduce the gap in budgets. Importantly, these differences
377 explained the minor deviation in the distributions of global budget partitioning into hemispheres
378 between INV_{AB} and TRENDY S3 (Fig. 3c). The differences between budget estimates for East Asia are
379 largely responsible for INV_{AB} indicating a stronger net sink in NE lands than TRENDY S3. Likewise,
380 the differences in the estimates for South America are responsible for the INV_{AB} indicating a stronger
381 net source in ST lands than those of TRENDY S3. Thus, East Asia and South America are the regions
382 where future model improvements are needed to generate CO₂ budgets that agree at the hemispheric and
383 regional scales.



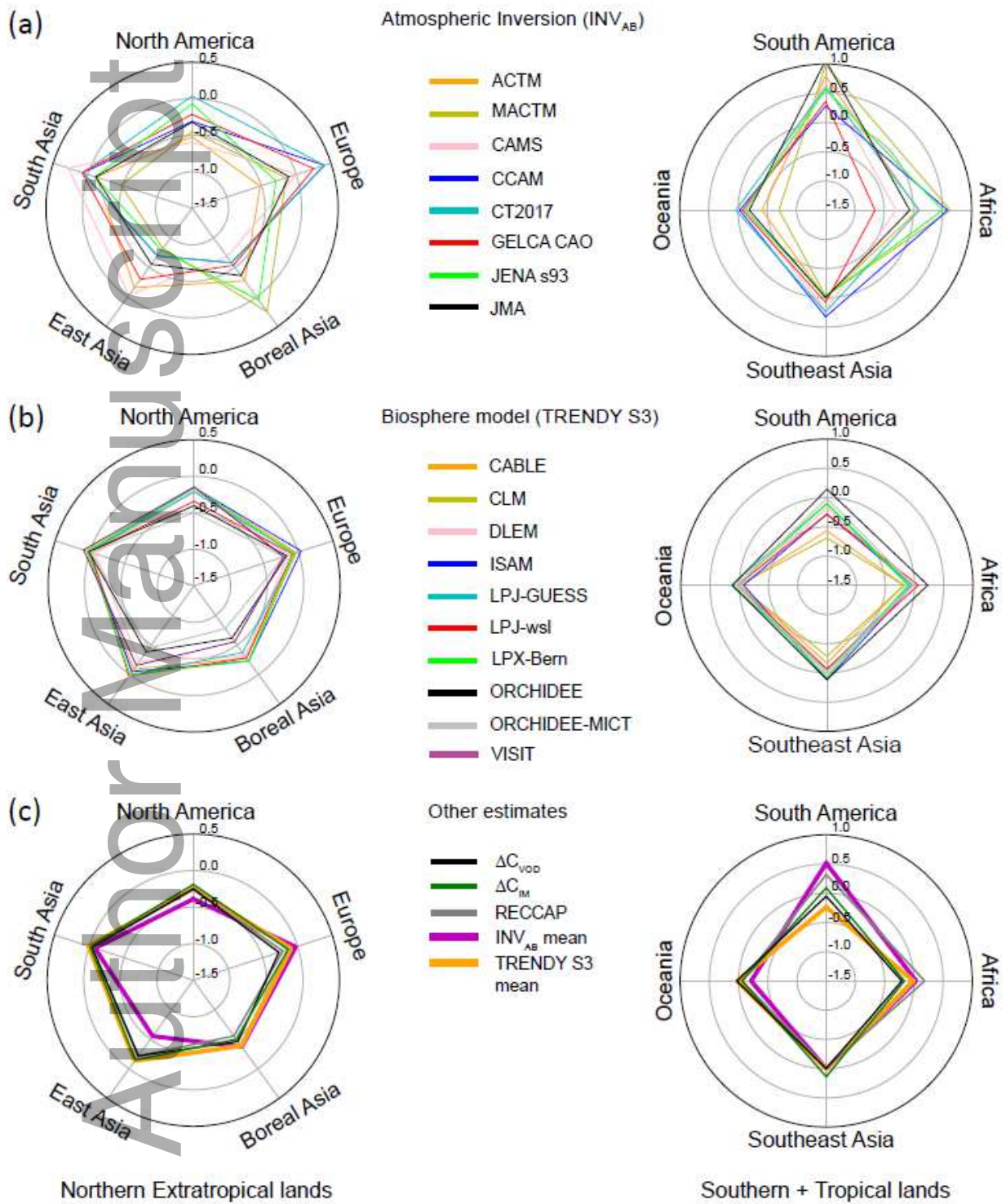
384

385 **FIGURE 5.** Consistency and inconsistency among the estimates of regional CO₂ budgets. Regional CO₂ budgets
 386 for the 2000s by the biosphere models (TRENDY S2 and S3) and atmospheric inversions (INV and INV_{AB}),
 387 carbon stock changes (ΔC_{VOD} and ΔC_{IM}), and RECCAP project. Regional classification is based on the RECCAP
 388 studies. Colors and symbols are the same as in Figure 3a.

389

390 So far, we evaluated the regional CO₂ budgets in terms of the average patterns of the atmospheric
 391 inversions and biosphere models. However, to derive robust budget agreements for all regions, the
 392 means by which individual models partitioned hemispheric budgets into the nine regions must be further
 393 investigated. Contrary to the consistent pattern found in the global budget partitioning, individual INV_{AB}
 394 results showed largely different patterns for the partitioning of NE and ST land budgets (Fig. 6a). Some
 395 inversions showed a greater net source or reduced sink in Europe, corresponding to a greater net sink in
 396 boreal Asia, while others showed the opposite pattern between these two regions. This sink-source
 397 compensation was also identified between boreal Asia and East Asia, East Asia and South Asia, and
 398 South America and Africa, with large variabilities in their patterns. These results suggest that differences
 399 in the sink-source compensation are likely the major factor responsible for the large range found in
 400 regional budget estimates by INV_{AB} (Fig. 5). Although the magnitudes of budgets differed, the pattern of
 401 NE and ST land budget partitioning was overall similar among the models of TRENDY S3 (Fig. 6b).

402 Additionally, ΔC_{VOD} , ΔC_{IM} , and RECCAP showed close agreements in their patterns of partitioning (Fig.
 403 6c), more closely resembling the average pattern of TRENDY S3 than that of INV_{AB} .



404
 405 **FIGURE 6.** Multi-method comparison of hemispheric budget partitioning into regions. Partitioning of
 406 hemispheric budgets into corresponding regions by **a)** INV_{AB} , **b)** TRENDY S3, and **c)** means of INV_{AB} and

407 TRENDY S3, and other independent estimates (ΔC_{IM} , ΔC_{VOD} , and RECCAP). Partitioning of the NE land budget
408 into five regions and the ST land budget into four regions are shown for each method. All figures are in units of
409 Pg C yr⁻¹.

410

411 **5. CHALLENGES FOR ESTIMATING REGIONAL CO₂ BUDGETS**

412 Schimel, Stephens, and Fisher (2015) demonstrated a rough agreement in the global budget
413 partitioning between atmospheric inversions that are capable of reproducing the observed annual vertical
414 gradients of atmospheric CO₂ and biosphere models that simulate offsets between the CO₂ and LUC
415 effects. The results of our study revealed that agreements between the latest atmospheric inversions and
416 biosphere models are more consistent under a unified definition of the net CO₂ flux (Fig. 3c), confirming
417 the roles of NE and ST lands in the global carbon cycle (Gaubert et al., 2019; Schimel, Stephens, &
418 Fisher, 2015; Stephens et al., 2007). However, our results also emphasize that this level of agreement is
419 insufficient to fully reconcile regional CO₂ budgets, as illustrated in Figure 5. In addition, a meta-
420 analysis of individual estimates from TRENDY S3 and INV_{AB} indicates that the agreement between
421 individual models found for particular regions does not necessarily hold true for the other regions (Fig.
422 S5). This implies that we do not yet have an optimal combination of atmospheric inversions and
423 biosphere models that is capable of producing consistent budget estimates for all global regions. To
424 achieve consistent global, hemispheric, and regional CO₂ budgets between the two methods, we need to
425 acknowledge some fundamental issues in modeling that should be resolved in future studies.

426 To produce regional CO₂ budgets with lower uncertainties, differences in the sink-source
427 compensation (“the dipole effect”; Peylin, Baker, Sarmiento, Ciais, & Bousquet, 2002) among
428 individual inversions need to be reduced. The dipole effect is intrinsic to the design of inversion systems,
429 where the CO₂ budgets of neighboring regions connected via wind paths are tightly anti-correlated,
430 because the sum of the regions is better constrained from the large-scale atmospheric signals than the
431 individual regions. Europe and boreal Asia are a good example of this effect, with both exhibiting large
432 variability, but a reverse order in the net sinks and sources of individual inversions (Fig. 6). While
433 additional CO₂ observations could provide better constraints of the inversion system at global regions,
434 this alone is unlikely to resolve the large variability among inversions. As notable variability was found
435 in Europe, one of the regions characterized by a high density of in-situ CO₂ observations, we need to
436 acknowledge a possibility that modeling issues are responsible for this variability. They include
437 differences in prior datasets, model resolution, control vector size (a set of posterior CO₂ fluxes to be

438 estimated at given temporal and spatial resolutions), assimilation window length (the period during
439 which data assimilation is conducted), transport rates (rates at which CO₂ is transported from a source
440 region to neighboring regions through model atmosphere), and transport model errors (in particular
441 concerning vertical mixing) among inversions. For example, the degree to which a regional budget
442 reflects localized fossil fuel signals or CO₂ measurement signals varies with the resolution of the
443 transport models and the size of the inversion control vector. These differences might have caused the
444 large variability in the European CO₂ budgets, which then propagated into the budget estimates for
445 boreal Asia via the dipole effect. Recent studies highlighted uncertainties in inter-hemispheric CO₂
446 transports as one of the causes behind the variability in zonal CO₂ budgets among inversions (Le Quéré
447 et al., 2018b; Schuh et al., 2019). The variability co-occurring between neighboring regions indicates a
448 possibility that a non-negligible level of uncertainties may exist in intra-hemispheric transports as well.

449 Contrary to atmospheric inversions, the biosphere models produced a relatively consistent pattern of
450 hemispheric budget partitioning (Fig. 6b), however, this does not mean that the results are more reliable.
451 Biosphere models still poorly represent certain processes, such as forest regrowth, cropland harvesting
452 and management, shifting cultivation, wood harvesting, and degradation (Arneeth et al., 2017; Kondo et
453 al., 2018b; Mitchard, 2018; Pugh et al. 2015, 2019; Williams, Gu, MacLean, Masek, & Collatz, 2016;
454 Wolf et al., 2015), which could greatly affect regional budget estimates. For instance, a recent model
455 that integrated the global forest age (the global forest age dataset (GFAD): Poulter et al., 2019)
456 suggested the enhancement of CO₂ uptake (~0.45 Pg C yr⁻¹) by regrowth of northern temperate and
457 boreal forests (Pugh et al., 2019), compared with simulations without the age information. Although this
458 alone may not resolve the issue, enhanced uptake by the age effect appears to play a role in filling the
459 gap between the atmospheric inversions and biosphere models in East Asia (Fig. 5), as this region is one
460 of the hot-spots of forest regrowth (Kondo et al., 2018a). In the case of South America, incomplete
461 representations of shifting cultivation, wood harvesting, and forest degradation are potential causes for
462 the biosphere models being inclined towards a net sink, opposite to the results based on atmospheric
463 inversions (Fig. 5). Currently, there is limited spatiotemporal information available regarding forest
464 degradation, but several studies have suggested that forest degradation is more important than other
465 processes in tropical regions, potentially accounting for twice the carbon release of deforestation
466 (Baccini et al., 2017; Mitchard, 2018; Ryan, Berry, & Joshi, 2014). Additional sinks and sources from
467 these processes are expected to change the patterns of hemispheric budget partitioning and
468 corresponding regional CO₂ budgets in the biosphere models of this study. Furthermore, although the

469 spread in regional budget estimates was smaller within the biosphere models than the atmospheric
470 inversions, spread in seasonality of net CO₂ flux was larger within the biosphere models than the
471 atmospheric inversions across global, hemispheric, and regional scales (Fig. S6). Thus, we cannot
472 conclude that biosphere models are more reliable than atmospheric inversions based on the consistency
473 of the hemispheric budget partition and regional budget estimates among models.

474 A tendency for ΔC_{IM} , ΔC_{VOD} , and RECCAP results to agree more with biosphere models in
475 estimates of regional budgets and partitioning than with atmospheric inversions may suggest that they
476 capture common signals within the carbon cycle (Figs. 5, 6). However, we need to acknowledge the fact
477 that carbon stock changes based on inventory measurements and VOD, as well as the statistical
478 approaches of RECCAP have their own limitations. Both ΔC_{IM} and ΔC_{VOD} provide "forest-oriented"
479 CO₂ budgets as available inventory data are of forests in large part and the conversion of VOD to
480 biomass was based on an empirical relationship using ground measurements of forest biomass (Liu et al.,
481 2015). These are considered insufficient to represent the diversity of terrestrial ecosystems, which
482 include grasslands and croplands, and their associated carbon fluxes (King et al., 2015). Uncertainty in
483 soil carbon stocks also affects the estimation of carbon stock changes. Even in the most extensive
484 compilation of the inventory data, the global soil carbon stocks are likely underestimated, due to missing
485 data of deep organic soils in ecosystems such as peatlands and mangroves (Pan et al., 2011). Despite
486 efforts to integrate possible processes in the carbon cycle for each region, the regional CO₂ budgets from
487 RECCAP are also influenced by the limitations in the independent CO₂ fluxes used for budget
488 assessment, including the above-mentioned limitations in atmospheric inversions, biosphere models, and
489 inventories. Thus, along with the modeling methods, ΔC_{IM} , ΔC_{VOD} , and the statistical approaches of
490 RECCAP should also be improved to serve as good references for future model improvements.

491 In addition to the above-mentioned issues of each method, further adjustments for the definition of
492 the net CO₂ flux could reduce the gap in budget estimates between the modeling methods. For instance,
493 lateral transports of harvested wood carbon via export and import affect regional CO₂ budget estimates
494 (Peters, Davis, & Andrew, 2012), which is not well addressed in current biosphere models. Also,
495 incorporation of bottom-up pathways of CO₂ resulting from oxidation of biogenetic volatile organic
496 compounds (BVOC), CO, CH₄ (e.g., coming from biosphere, fire and fossil fuel emissions) could
497 improve the gap in budget estimates. Despite recent progress aimed at filling the gaps between
498 atmospheric inversions and biosphere models, our current level of modeling and process understanding
499 is still insufficient to implement these factors into the multi-scale CO₂ budget comparison.

500

501 **6. CONCLUSIONS**

502 The aim of this study was to detail the current status of agreement between terrestrial CO₂ budgets
503 derived from top-down and bottom-up approaches and to provide a pathway for future improvement of
504 these methods. With comparisons under a consistent definition of net CO₂ flux, we illustrated different
505 levels of consistency in the CO₂ budgets of atmospheric inversions and biosphere models at the global,
506 hemispheric, and regional scales. The overlapping distributions of hemispheric budgets, and close
507 agreement found for some regions (i.e., North America and Southeast Asia) are good indications of
508 progress towards reconciliation of budget estimates, therefore, increasing robustness of our knowledge.
509 However, further improvements are required to reach a more robust regional understanding.

510 First, differences in budget estimates between the modeling methods for East Asia and South
511 America need to be reduced. To accomplish this, the impacts of physiological processes that contribute
512 to net sinks or sources (e.g., age effects on regrowth, degradation, etc.) should be further investigated
513 using biosphere models. Second, the large variability in the regional dipole effect within atmospheric
514 inversions needs to be reduced for them to be more comparable with the estimates of biosphere models.
515 This requires collective effort from the inverse modeling community to identify and resolve modeling
516 issues at regional scales (e.g., detailed experiments on transport model and inversion performance,
517 validation of fossil fuel and biogenetic flux partitioning using ¹⁴CO₂ measurements, etc.). Given these
518 findings, caution should be taken when interpreting regional CO₂ budgets estimated using only either
519 atmospheric inversions or biosphere models, or individual models from these approaches, unless
520 regional applications have been properly parameterized and benchmarked with regional observations.

521 The terrestrial biosphere plays a major role in mitigating CO₂ emitted by human activities (Le Quéré
522 et al., 2018b). While the partitioning of the sink between the northern hemisphere and pantropic is
523 increasingly better constrained, we have yet to establish confidence in the roles of global regions
524 because of the uncertainties remaining in current models. Those uncertainties continue to limit our
525 ability to project the mitigation potential by the terrestrial biosphere (Hoffman et al., 2014), and require
526 continuous international and multidisciplinary efforts to resolve such as those under the umbrella of the
527 Global Carbon Project.

528

529 **Acknowledgements**

530 This paper is a contribution to the REgional Carbon Cycle Assessment and Processes (RECCAP) under
531 the umbrella of the Global Carbon Project. M. Kondo, P.K. Patra, K. Ichii, T. Maki, and T. Saeki
532 acknowledge support from Environment Research and Technology Development Funds of the
533 Environmental Restoration and Conservation Agency of Japan (no. 2-1701), P.K. Patra and J.G.
534 Canadell from Asia-Pacific Network for Global Change Research (ARCP2011-11NMY-Patra/Canadell),
535 P. Friedlingstein from the CRESCENDO project that received funding from the European Union's
536 Horizon 2020 research and innovation program (no. 641816), P. Friedlingstein and S. Lienert from the
537 CCICC project that received funding from the European Union's Horizon 2020 research and innovation
538 program (no. 821003), A. Bastos from the European Space Agency Climate Change Initiative ESA-CCI
539 RECCAP2 project (ESRIN/4000123002/18/I-NB), A. Arneth and P. Anthoni from the German
540 Helmholtz Association in its ATMO programme, M. Kautz from the European Union FP7 project
541 LUC4C (no. 603542), R. Lauerwald from the VERIFY project that received funding from the European
542 Union's Horizon 2020 research and innovation program (no. 776186), A.K. Jain from Department of
543 Energy (no. DE-SC0016323) and National Science Foundation: NSF (no. NSF AGS 12-43071), H. Tian
544 from NSF (no. 1243232), and J.G. Canadell, V. Haverd, T. Ziehn from the Australian National
545 Environmental Science Program-Earth Systems and Climate Change Hub. CLM is a part of the CESM
546 project that is supported primarily by NSF. This material is based upon work supported by the National
547 Center for Atmospheric Research, which is a major facility sponsored by the NSF under Cooperative
548 Agreement No. 1852977. Computing and data storage resources, including the Cheyenne supercomputer
549 (doi:10.5065/D6RX99HX), were provided by the Computational and Information Systems Laboratory
550 (CISL) at NCAR. We thank all the scientists, software engineers, and administrators who contributed to
551 the development of CESM2.

552

553 **Data availability:** TRENDY data are available via Profs. Stephen Sitch and Pierre Friedlingstein,
554 Exeter University (s.a.sitch@exeter.ac.uk; p.friedlingstein@exeter.ac.uk). CAMS, CT2017, JENA
555 inversion data are available from the web sites (CAMS: [https://apps.ecmwf.int/datasets/data/cams-ghg-](https://apps.ecmwf.int/datasets/data/cams-ghg-inversions/)
556 [inversions/](https://apps.ecmwf.int/datasets/data/cams-ghg-inversions/), CT2017: <https://www.esrl.noaa.gov/gmd/ccgg/carbontracker/>, JENA: [http://www.bgc-](http://www.bgc-jena.mpg.de/CarboScope/)
557 [jena.mpg.de/CarboScope/](http://www.bgc-jena.mpg.de/CarboScope/)). ACTM, MACTM, CCAM, and GELCA CAO inversion data are available
558 by contacting Dr. Prabir K. Patra (prabir@jamstec.go.jp). JMA inversion data are available by
559 contacting Dr. Takashi Maki (tmaki@mri-jma.go.jp). Global above-ground biomass carbon (v1.0) is
560 available from the web site (http://wald.anu.edu.au/data_services/data/global-above-ground-biomass-

561 carbon-v1-0/). Flux data of Global Carbon Project are available from the web site
562 (<https://www.globalcarbonproject.org/carbonbudget/18/data.htm>).

563

564 **Competing interests:** The authors declare that there are no competing financial interests

Author Manuscript

565 **REFERENCES**

- 566 Arneth, A., Sitch, S., Pongratz, J., Stocker, B.D., Ciais, P., Poulter, B., ... Zaehle, S. (2017). Historical
567 carbon dioxide emissions caused by land-use changes are possibly larger than assumed. *Nature*
568 *Geoscience*, 10(2), 79–84. doi: 10.1038/ngeo2882
- 569 Baccini, A., Walker, W., Carvalho, L., Farina, M., Sulla-Menashe, D., & Houghton, R.A. (2017).
570 Tropical forests are a net carbon source based on aboveground measurements of gain and loss.
571 *Science*, 358(6360), 230–234. doi: 10.1126/science.aam5962
- 572 Ballantyne, A.P., Andres, R., Houghton, R., Stocker, B.D., Wanninkhof, R., Anderegg, W., ... White,
573 J.W.C. (2015). Audit of the global carbon budget: Estimate errors and their impact on uptake
574 uncertainty. *Biogeosciences*, 12(8), 2565–2584. doi: 10.5194/bg-12-2565-2015
- 575 Canadell, J.G., Ciais, P., Gurney, K., Le Quéré, C., Piao, S., Raupach, M.R., & Sabine, C.L. (2011). An
576 international effort to quantify regional carbon fluxes. *Eos Transactions American Geophysical*
577 *Union*, 92(10), 81–82. doi: 10.1029/2011EO100001
- 578 Cervarich, M., Shu, S., Jain, A.K., Arneth, A., Canadell, J., Friedlingstein, P., ... Zeng, N. (2016). The
579 Terrestrial Carbon budget of South and Southeast Asia. *Environmental Research Letters*, 11,
580 doi:10.1088/1748-9326/11/10/105006
- 581 Ciais, P., Sabine, C., Bala, G., Bopp, L., Brovkin, V., Canadell, J., ... Thornton, P. (2013). Carbon and
582 other biogeochemical cycles. In: T.F. Stocker, D. Qin, G.-K. Plattner, M. Tignor, S.K. Allen, J.
583 Boschung, ... P.M. Midgley (Eds.), *Climate Change 2013: The Physical Science Basis, Contribution*
584 *of Working Group I to the Fifth Assessment Report of the Intergovernmental Panel on Climate*
585 *Change* (pp. 465–570). Cambridge: Cambridge University Press.
- 586 Ciais, P., Tan, J., Wang, X., Roedenbeck, C., Chevallier, F., Piao, S.-L., ... Tans, P. (2019). Five decades
587 of northern land carbon uptake revealed by the interhemispheric CO₂ gradient. *Nature*, 568(7751),
588 221–225. doi: 10.1038/s41586-019-1078-6
- 589 Chevallier, F., Ciais, P., Conway, T.J., Aalto, T., Anderson, B.E., Bousquet, P., ... Worthy, D. (2010).
590 CO₂ surface fluxes at grid point scale estimated from a global 21 year reanalysis of atmospheric
591 measurements. *Journal of Geophysical Research: Atmospheres* 115, D21307. doi:
592 10.1029/2010JD013887

- 593 Friedlingstein, P., Cox, P., Betts, R., Bopp, L., von Bloh, W., Brovkind, V., ... Zeng, N. (2006). Climate-
594 carbon cycle feedback analysis: results from the C4MIP model intercomparison. *Journal of Climate*,
595 19, 3337–3353. doi:10.1175/JCLI3800.1
- 596 Food and Agriculture Organization, Global forest resources assessment 2005 (Forestry Paper 147, Food
597 and Agriculture Organization, Rome, 2006). [http://www.fao.org/forest-resources-assessment/past-](http://www.fao.org/forest-resources-assessment/past-assessments/fra-2005/en/)
598 [assessments/fra-2005/en/](http://www.fao.org/forest-resources-assessment/past-assessments/fra-2005/en/)
- 599 Food and Agriculture Organization, Global forest resources assessment 2010 (Forestry Paper 163, Food
600 and Agriculture Organization, Rome, 2010). [http://www.fao.org/forest-resources-assessment/past-](http://www.fao.org/forest-resources-assessment/past-assessments/fra-2010/en/)
601 [assessments/fra-2010/en/](http://www.fao.org/forest-resources-assessment/past-assessments/fra-2010/en/)
- 602 Gaubert, B., Stephens, B.B., Basu, S., Chevallier, F., Deng, F., Kort, E.A., ... Yin, Y. (2019). Global
603 atmospheric CO₂ inverse models converging on neutral tropical land exchange, but disagreeing on
604 fossil fuel and atmospheric growth rate. *Biogeosciences*, 16(1), 117–134. doi: 10.5194/bg-16-117-
605 2019
- 606 Guimberteau, M., Zhu, D., Maignan, F., Huang, Y., Yue, C., Dantec-Nédélec, S., ... Ciais, P. (2018)
607 ORCHIDEE-MICT (v8.4.1), a land surface model for the high latitudes: Model description and
608 validation. *Geoscientific Model Development*, 11(1), 121–163. doi: 10.5194/gmd-11-121-2018
- 609 Gurney, K.R., Law, R.M., Denning, A.S., Rayner, P.J., Baker, D., Bousquet, P., ... Yuen, C.-W. (2002).
610 Towards robust regional estimates of CO₂ sources and sinks using atmospheric transport models.
611 *Nature*, 415(6872), 626–630. doi: 10.1038/415626a
- 612 Haverd, V., Smith, B., Nieradzick, L., Briggs, P.R., Woodgate, W., Trudinger, C.M., ... Cuntz, M. (2018).
613 A new version of the CABLE land surface model (Subversion revision r4601) incorporating land
614 use and land cover change, woody vegetation demography, and a novel optimisation-based
615 approach to plant coordination of photosynthesis. *Geoscientific Model Development*, 11(7), 2995–
616 3026. doi: 10.5194/gmd-11-2995-2018
- 617 Hoffman, F.M., Randerson, J.T., Arora, V.K., Bao, Q., Cadule, P., Ji, D., ... Wu, T. (2014). Causes and
618 implications of persistent atmospheric carbon dioxide biases in Earth System Models. *Journal of*
619 *Geophysical Research: Biogeosciences*, 119(2), 141–162. doi:10.1002/2013JG002381
- 620 Houghton, R. A. (2007) Balancing the global carbon budget. *Annual Review of Earth and Planetary*
621 *Science*, 35, 313-347. doi:10.1146/annurev.earth.35.031306.140057

- 622 Hurtt, G., Chini, L., Sahajpal, R., Frohking, S., Calvin, K., Fujimori, S., ... Lawrence, P. (2017).
623 Harmonization of global land-use change and management for the period 850–2100. (Online).
624 luh.umd.edu/data.shtml
- 625 Iida, Y., Kojima, A., Takatani, Y., Nakano, T., Sugimoto, M., Midorikawa, T., Ishii, M. (2015). Trends
626 in $p\text{CO}_2$ and sea-air CO_2 flux over the global open oceans for the last two decades. *Journal of*
627 *Oceanography*, 71(6), 637–661. doi:10.1007/s10872-015-0306-4
- 628 Jacobson, A.R., Fletcher, S.E.M., Gruber, N., Sarmiento, J.L., & Gloor, M. (2007). A joint
629 atmosphere - ocean inversion for surface fluxes of carbon dioxide: 1. Methods and global-scale
630 fluxes. *Global Biogeochemical Cycles*, 21(1), GB1019. doi: 10.1029/2005GB002556
- 631 Jain, A.K., Meiyappan, P., Song, Y., & House, J.I. (2013). CO_2 emissions from land-use change affected
632 more by nitrogen cycle, than by the choice of land-cover data. *Global Change Biology*, 19(9), 2893–
633 2906. doi: doi.org/10.1111/gcb.12207
- 634 Kaula, M., Dadhwal, V.K., Mohren, G.M.J. (2009). Land use change and net C flux in Indian forests.
635 *Forest Ecology and Management*, 258, 2(15), 100-108. doi:10.1016/j.foreco.2009.03.049
- 636 Kato, E., Kinoshita, T., Ito, A., Kawamiya, M., & Yamagata, Y. (2013). Evaluation of spatially explicit
637 emission scenario of land-use change and biomass burning using a process-based biogeochemical
638 model. *Journal of Land Use Science*, 8(1), 104–122. doi: 10.1080/1747423X.2011.628705
- 639 Keeling, R.F. & Manning, A.C. (2014). Studies of recent changes in atmospheric O_2 content. In: H.D.
640 Holland & K.K. Turekian (Eds.) *Treatise on Geochemistry* (2nd ed.) (pp. 385–404). Amsterdam:
641 Elsevier.
- 642 Keenan, T.F., Prentice, I.C., Canadell, J.G., Williams, C.A., Wang, H., Raupach, M., & Collatz, G.J.
643 (2016). Recent pause in the growth rate of atmospheric CO_2 due to enhanced terrestrial carbon
644 uptake. *Nature Communications*, 7, 13428. doi: 10.1038/ncomms13428
- 645 Keenan, T.F., & Williams, C.A. (2018). The terrestrial carbon sink. *Annual Review of Environment and*
646 *Resources*, 43, 219–43. doi: 10.1146/annurev-environ-102017-030204
- 647 Keller, K.M., Lienert, S., Bozbiyik, A., Stocker, T.F., Churakova (Sidorova), O.V., Frank, D.C., ... Joos,
648 F. (2017). 20th century changes in carbon isotopes and water-use efficiency: tree-ring-based

649 evaluation of the CLM4.5 and LPX-Bern models. *Biogeosciences*, 14, 2641-2673. doi:10.5194/bg-
650 14-2641-2017

651 King, A.W., Andres, R.J., Davis, K.J., Hafer, M., Hayes, D.J., Huntzinger, D.N., ... Woodall, C.W.
652 (2015). North America's net terrestrial CO₂ exchange with the atmosphere 1990–2009.
653 *Biogeosciences*, 12(2), 399–414. doi: 10.5194/bg-12-399-2015

654 Klein Goldewijk, K., Beusen, A., Doelman, J., & Stehfest, E. (2017). Anthropogenic land use estimates
655 for the Holocene – HYDE 3.2. *Earth System Scientific Data*, 9, 927–953. doi: 10.5194/essd-9-927-
656 2017

657 Kondo, M., Ichii, K., Takagi, H., & Sasakawa, M. (2015). Comparison of the data-driven top-down and
658 bottom-up global terrestrial CO₂ exchanges: GOSAT CO₂ inversion and empirical eddy flux
659 upscaling. *Journal of Geophysical Research: Biogeosciences*, 120(7), 1226–1245. doi: 10.1002/
660 2014JG002866

661 Kondo, M., Ichii, K., Patra, P.K., Poulter, B., Calle, L., Koven, C., ... Wiltshire, A. (2018a). Plant
662 regrowth as a driver of recent enhancement of terrestrial CO₂ uptake. *Geophysical Research Letters*,
663 45(10), 4820–4830. doi: 10.1029/2018GL077633

664 Kondo, M., Ichii, K., Patra, P.K., Canadell, J.G., Poulter, B., Sitch, S., ... Rödenbeck, C. (2018b). Land
665 use change and El Niño-Southern Oscillation drive decadal carbon balance shifts in Southeast Asia.
666 *Nature Communications*, 9, 1154. doi: 10.1038/s41467-018-03374-x

667 Krinner, G., Viovy, N., de Noblet-Ducoudré, N., Ogée, J., Polcher, J., Friedlingstein, P., ... Prentice,
668 I.C. (2005). A dynamic global vegetation model for studies of the coupled atmosphere biosphere
669 system. *Global Biogeochemical Cycles*, 19(1), 1–33. doi: 10.1029/2003GB002199

670 Lauerwald, R., Laruelle, G.G., Hartmann, J., Ciais, P., & Regnier, P.A.G. (2015). Spatial patterns in
671 CO₂ evasion from the global river network. *Global Biogeochemical Cycles*, 29(5), 534–554. doi:
672 10.1002/2014GB004941

673 Le Quéré, C., Andrew, R.M., Friedlingstein, P., Sitch, S., Pongratz, J., Manning, A.C., ... Zhu, D.
674 (2018a). Global Carbon Budget 2017. *Earth System Scientific Data*, 10, 405-448. doi:10.5194/essd-
675 10-405-2018

- 676 Le Quéré, C., Andrew, R.M., Friedlingstein, P., Sitch, S., Hauck, J., Pongratz, J., ... Zheng, B. (2018b).
677 Global Carbon Budget 2018. *Earth System Scientific Data*, 10(4), 2141–2194. doi: 10.5194/essd-
678 10-2141-2018
- 679 Li, W., Ciais, P., Wang, Y., Peng, S., Broquet, G., Ballantyne, A.P., ... Pongratz, J. (2016). Reducing
680 uncertainties in decadal variability of the global carbon budget with multiple datasets. *Proceedings*
681 *of the National Academy of Sciences*, 113(46), 13104–13108. doi: 10.1073/pnas.1603956113
- 682 Liu, Y.Y., van Dijk, A.I.J.M., de Jeu, R.A.M., Canadell, J.G., McCabe, M.F., Evans, J.P., & Wang, G.
683 (2015). Recent reversal in loss of global terrestrial biomass. *Nature Climate Change*, 5(5), 470–474.
684 doi: 10.1038/nclimate2581
- 685 Maki, T., Ikegami, M., Fujita, T., Hirahara, T., Yamada, K., Mori, K., ... Conway, T.J. (2010). New
686 technique to analyse global distributions of CO₂ concentrations and fluxes from non-processed
687 observational data. *Tellus B: Chemical and Physical Meteorology*, 62(5), 797–809. doi:
688 10.1111/j.1600-0889.2010.00488.x
- 689 Mayorga, E., Seitzinger, S. P., Harrison, J. A., Dumont, E., Beusen, A. H. W., Bouwmand, A. F., ...
690 Drecht, G. V. (2010). Global Nutrient Export from WaterSheds 2 (NEWS 2): Model development
691 and implementation. *Environmental Modeling & Software*, 25, 837-853. doi:
692 10.1016/j.envsoft.2010.01.007
- 693 McGregor, J.L., & Dix, M.R. (2008). An updated description of the conformal cubic atmospheric model.
694 In: K. Hamilton & W. Ohfuchi (Eds.) *High Resolution Numerical Modeling of the Atmosphere and*
695 *Ocean* (pp. 51–76). Berlin: Springer.
- 696 Mitchard, E.T.A. (2018). The tropical forest carbon cycle and climate change. *Nature*, 559(7715), 527–
697 534. doi: 10.1038/s41586-018-0300-2
- 698 Oleson, K.W., Lawrence, D.M., Bonan, G.B., Drewniak, B., Huang, M., Koven, C.D., ... Thornton, P.E.
699 (2013). *Technical Description of Version 4.5 of the Community Land Model (CLM)*, National
700 Center for Atmospheric Research Technical Note. Boulder: NCAR. doi: 10.5065/D6RR1W7M
- 701 Pan, Y., Birdsey, R.A., Fang, J., Houghton, R., Kauppi, P.E., Kurz, W.A., ... Hayes, D. (2011). A large
702 and persistent carbon sink in the world's forests. *Science*, 333(6045), 988–993. doi:
703 10.1126/science.1201609

- 704 Patra, P. K., Takigawa, M., Watanabe, S., Chandra, N., Ishijima, K., Yamashita, Y. (2018). Improved
705 Chemical Tracer Simulation by MIROC4.0-based Atmospheric Chemistry-Transport Model
706 (MIROC4-ACTM). SOLA, 14, 91-96. doi:10.2151/sola.2018-016
- 707 Peters, G. P., Davis, S. J., & Andrew, R. (2012). A synthesis of carbon in international trade.
708 Biogeosciences, 9, 3247–3276. doi: 10.5194/bg-9-3247-2012
- 709 Peters, W., Jacobson, A.R., Sweeney, C., Andrews, A.E., Conway, T.J., Masarie, K., ... Tans, P.P.
710 (2007). An atmospheric perspective on North American carbon dioxide exchange: CarbonTracker.
711 Proceedings of the National Academy of Sciences, 104(48), 18925–18930. doi:
712 10.1073/pnas.0708986104
- 713 Peylin, P., Baker, D., Sarmiento, J., Ciais, P., & Bousquet, P. (2002). Influence of transport uncertainty
714 on annual mean and seasonal inversions of atmospheric CO₂ data. Journal of Geophysical Research,
715 107(D19), 4385. doi: 10.1029/2001JD000857
- 716 Peylin, P., Law, R.M., Gurney, K.R., Chevallier, F., Jacobson, A.R., Maki, T., ... Zhang, X. (2013).
717 Global atmospheric carbon budget: results from an ensemble of atmospheric CO₂ inversions.
718 Biogeosciences, 10, 6699–6720. doi: 10.5194/bg-10-6699-2013
- 719 Poulter, B., Aragão, L., Andela, N., Bellassen, V., Ciais, P., Kato, T., ... Shvidenko, A. (2019). The
720 Global Forest Age dataset and its uncertainties (GFADv1.1). National Aeronautics and Space
721 Administration, PANGAEA (Online). doi: 10.1594/PANGAEA.897392
- 722 Pugh, T.A.M., Arneth, A., Olin, S., Ahlström, A., Bayer, A.D., Klein Goldewijk, K., ... Schurgers, G.
723 (2015). Simulated carbon emissions from land-use change are substantially enhanced by accounting
724 for agricultural management. Environmental Research Letters, 10(12), 124008. doi: 10.1088/1748-
725 9326/10/12/124008
- 726 Pugh, T.A.M., Lindeskog, M., Smith, B., Poulter, B., Arneth, A., Haverd, V., & Calle, L. (2019). Role
727 of forest regrowth in global carbon sink dynamics. Proceedings of the National Academy of
728 Sciences, 116(10), 4382–4387. doi: 10.1073/pnas.1810512116
- 729 Raymond, P. A., Hartmann, J., Lauerwald, R., Sobek, S., McDonald, C., ... Guth, P. (2013). Global
730 carbon dioxide emissions from inland waters. Nature, 503, 355–359. doi:10.1038/nature12760

- 731 Regnier, P., Friedlingstein, P., Ciais, P., Mackenzie, F.T., Gruber, N., Janssens, I.A., ... Thullner, M.
732 (2013). Anthropogenic perturbation of the carbon fluxes from land to ocean. *Nature Geoscience*, 6,
733 597–607. doi:10.1038/ngeo1830
- 734 Rödenbeck, C., Houweling, S., Gloor, M., & Heimann, M. (2003). Time-dependent atmospheric CO₂
735 inversions based on interannually varying tracer transport. *Tellus B: Chemical and Physical*
736 *Meteorology*, 55(2), 488–497. doi: 10.1034/j.1600-0889.2003.00033.x
- 737 Rödenbeck, C., Zaehle, S., Keeling, R., & Heimann, M. (2018). How does the terrestrial carbon
738 exchange respond to inter-annual climatic variations? A quantification based on atmospheric CO₂
739 data. *Biogeosciences*, 15(8), 2481–2498. doi: 10.5194/bg-15-2481-2018
- 740 Ryan, C.M., Berry, N.J. & Joshi, N. (2014). Quantifying the causes of deforestation and degradation and
741 creating transparent REDD+ baselines: A method and case study from central Mozambique.
742 *Applied Geography*, 53, 45–54. doi: 10.1016/j.apgeog.2014.05.014
- 743 Saatchi, S.S., Harris, N.L., Brown, S., Lefsky, M., Mitchard, E.T.A., Salas, W., ... Morel, A. (2011).
744 Benchmark map of forest carbon stocks in tropical regions across three continents. *Proceedings of*
745 *the National Academy of Sciences*, 108(24), 9899–9904. doi: 10.1073/pnas.1019576108
- 746 Saeki, T., & Patra, P.K. (2017). Implications of overestimated anthropogenic CO₂ emissions on East
747 Asian and global land CO₂ flux inversion. *Geoscience Letters*, 4(1), 9. doi: 10.1186/s40562-017-
748 0074-7
- 749 Schimel, D., Stephens, B.B., & Fisher, J.B. (2015). Effect of increasing CO₂ on the terrestrial carbon
750 cycle. *Proceedings of the National Academy of Sciences*, 112(2), 436–441. doi:
751 10.1073/pnas.1407302112
- 752 Schuh, A.E., Jacobson, A.R., Basu, S., Weir, B., Baker, D., Bowman, K., ... Palmer, P.I. (2019)
753 Quantifying the impact of atmospheric transport uncertainty on CO₂ surface flux estimates. *Global*
754 *Biogeochemical Cycles*, 33(4), 484–500. doi: 10.1029/2018GB006086
- 755 Sitch, S., Smith, B., Prentice, I.C., Arneth, A., Bondeau, A., Cramer, W., ... Venevsky, S. (2003).
756 Evaluation of ecosystem dynamics, plant geography and terrestrial carbon cycling in the LPJ
757 dynamic vegetation model. *Global Change Biology*, 9(2), 161–185. doi: 10.1046/j.1365-
758 2486.2003.00569.x

- 759 Sitch, S., Huntingford, C., Gedney, N., Levy, P.E., Lomas, M., Piao, S.L., ... Woodward, F.I. (2008).
760 Evaluation of the terrestrial carbon cycle, future plant geography and climate-carbon cycle
761 feedbacks using five Dynamic Global Vegetation Models (DGVMs). *Global Change Biology*,
762 14(9), 2015–2039. doi: 10.1111/j.1365-2486.2008.01626.x
- 763 Sitch, S., Friedlingstein, P., Gruber, N., Jones, S.D., Murray-Tortarolo, G., Ahlström, A., ... Myneni, R.
764 (2015). Recent trends and drivers of regional sources and sinks of carbon dioxide. *Biogeosciences*,
765 12(3), 653–679. doi: 10.5194/bg-12-653-2015
- 766 Smith, B., Wårlind, D., Arneth, A., Hickler, T., Leadley, P., Siltberg, J., & Zaehle, S. (2014).
767 Implications of incorporating N cycling and N limitations on primary production in an individual-
768 based dynamic vegetation model. *Biogeosciences*, 11, 2027–2054. doi: 10.5194/bg-11-2027-2014
- 769 Stephens, B.B., Gurney, K.R., Tans, P.P., Sweeney, C., Peters, W., Bruhwiler, L., ... Denning, A.S.
770 (2007). Weak northern and strong tropical land carbon uptake from vertical profiles of atmospheric
771 CO₂. *Science*, 316(5832), 1732–1735. doi: 10.1126/science.1137004
- 772 Thompson, R.L., Patra, P.K., Chevallier, F., Maksyutov, S., Law, R.M., Ziehn, T., ... Ciais, P. (2016).
773 Top-down assessment of the Asian carbon budget since the mid 1990s. *Nature Communications*, 7,
774 10724. doi: 10.1038/ncomms10724
- 775 Tian, H., Chen, G., Lu, C., Xu, X., Hayes, D.J., Ren, W., ... Wofsy, S.C. (2015). North American
776 terrestrial CO₂ uptake largely offset by CH₄ and N₂O emissions: Toward a full accounting of the
777 greenhouse gas budget. *Climatic Change*, 129(3–4), 413–426. doi: 10.1007/s10584-014-1072-9
- 778 Viovy, N. (2018). CRUNCEP Version 7 - Atmospheric forcing data for the Community Land Model.
779 Research Data Archive at the National Center for Atmospheric Research, Computational and
780 Information Systems Laboratory (Online). <http://rda.ucar.edu/datasets/ds314.3/>
- 781 Williams, C.A., Gu, H., MacLean, R., Masek, J.G., & Collatz, J. (2016). Disturbance and the carbon
782 balance of US forests: A quantitative review of impacts from harvests, fires, insects, and droughts.
783 *Global Planetary Change*, 143, 66–80. doi: 10.1016/j.gloplacha.2016.06.002
- 784 Wolf, J., West, T.O., Le Page, Y., Kyle, G.P., Zhang, X., Collatz, G.J., & Imhoff, M.L. (2015). Biogenic
785 carbon fluxes from global agricultural production and consumption. *Global Biogeochemical Cycles*,
786 29(10), 1617–1639. doi: 10.1002/2015GB005119

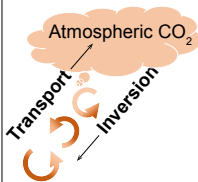
787 Zhuravlev, R., Khattatov, B., Kiryushov, B., & Maksyutov, S. (2011). A novel approach to estimation of
788 time-variable surface sources and sinks of carbon dioxide using empirical orthogonal functions and
789 the Kalman filter. *Atmospheric Chemistry and Physics*, 11(20), 10305–10315. doi: 10.5194/acp-11-
790 10305-2011

791 Zscheischler, J., Mahecha, M.D., Avitabile, V., Calle, L., Carvalhais, N., Ciais, P., ... Reichstein, M.
792 (2017). Reviews and syntheses: An empirical spatiotemporal description of the global surface–
793 atmosphere carbon fluxes: Opportunities and data limitations. *Biogeosciences*, 14, 3685–3703. doi:
794 10.5194/bg-14-3685-2017

Author Manuscript

Atmospheric inversion

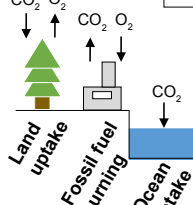
Net CO₂ flux between atmosphere and land estimated from atmospheric CO₂ measurements considering wind transport. Atmospheric inversion seeks an optimal solution from atmospheric CO₂ measurements and prior information, such as fossil fuel burning, fire emissions, and net land and ocean fluxes.



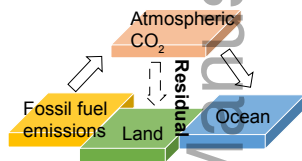
gcb_14917_f1.pdf

O₂-based method

Global net land CO₂ flux based on long-term measurements of atmospheric O₂ (in terms of O₂/N₂ ratio) and CO₂. Measurement data are fed into mathematical equations for construction and destruction of organic matters that exert the dominant control on the atmospheric O₂ and CO₂ variability.

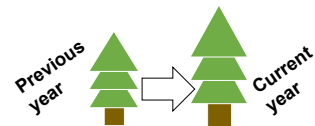


Residual method



Global net land CO₂ flux estimated as a residual of the difference between measurements of CO₂ growth rate, estimations of fossil fuel emissions, and atmosphere-ocean CO₂ exchange.

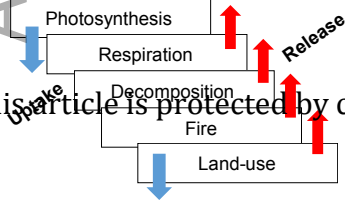
Carbon stock change



Vegetation optical depth (VOD)-based: annual carbon stock change based on successive VOD measurements from passive microwave sensors. Inventory-based: decadal carbon stock change based on regionally aggregated inventory measurements.

Net CO₂ flux

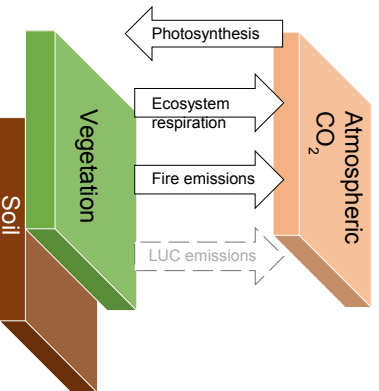
Biosphere model



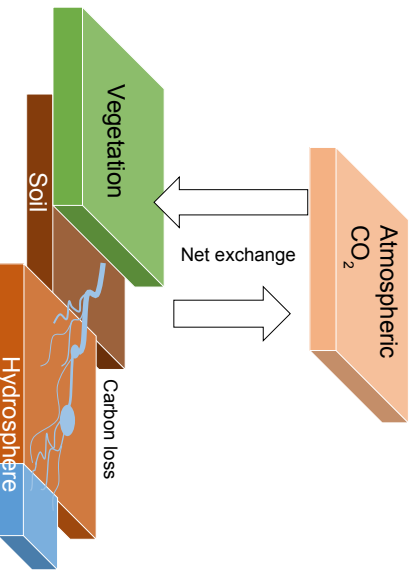
Net CO₂ flux as a sum of fluxes simulated under theoretical and semi-empirical bases. It considers processes of carbon uptake and release. All rights reserved. respiration, decomposition, land-use change emissions, and fire emissions, etc.

This article is protected by copyright. All rights reserved.

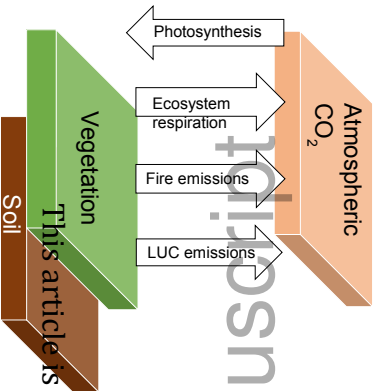
(a) TRENDY S2



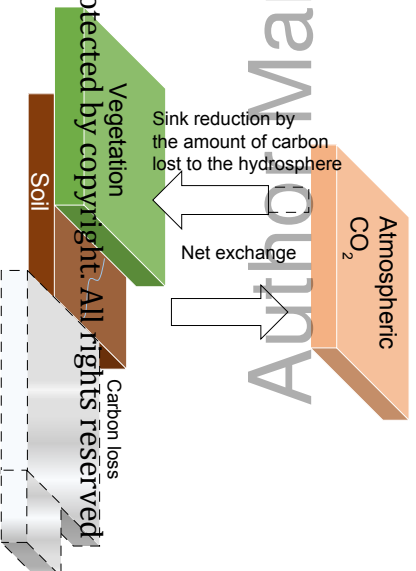
(b) INV



(c) TRENDY S3



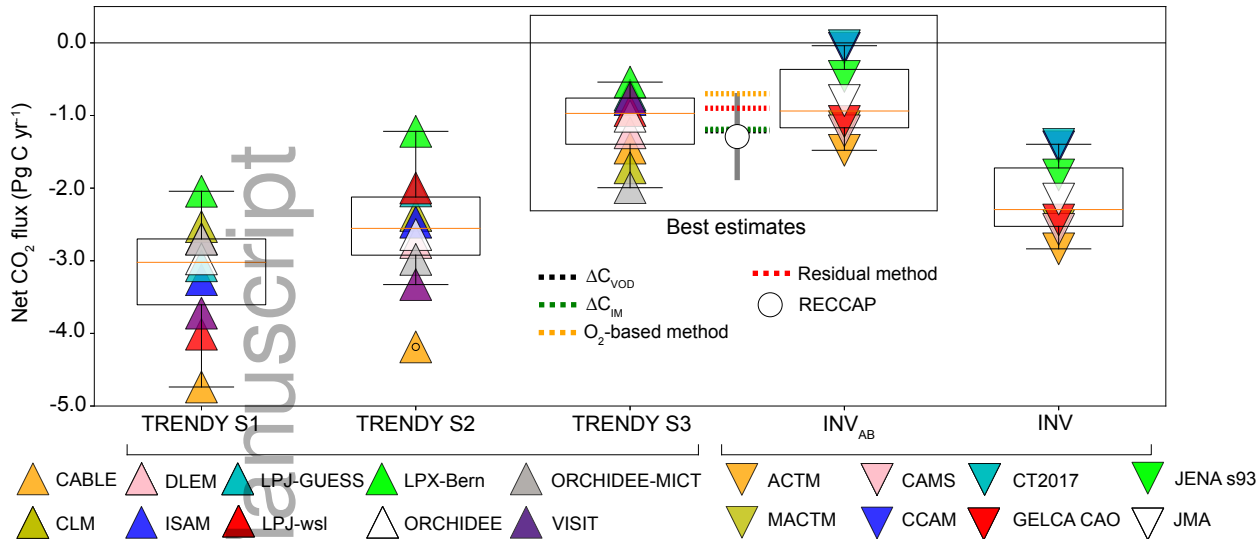
(d) INV_{AB}



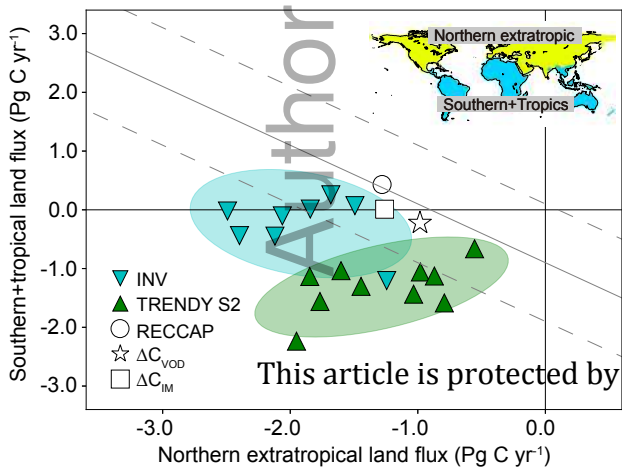
This article is protected by copyright. All rights reserved.

Author Manuscript

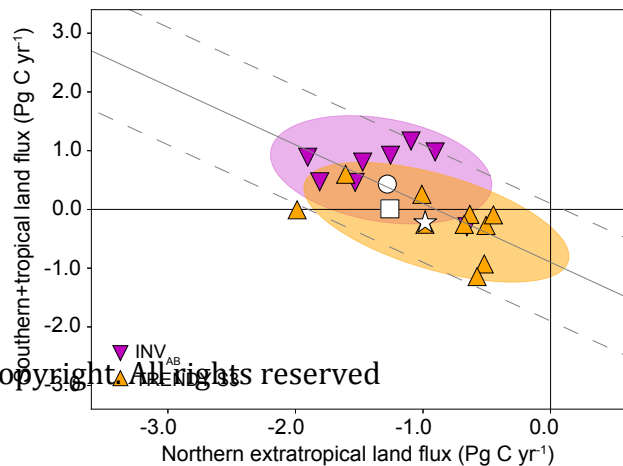
(a) gcb_14917_f3.pdf



(b) IPCC AR5 reproduction

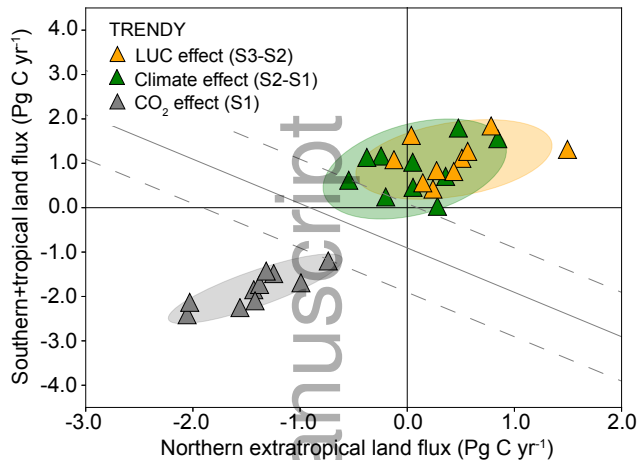


(c) This study

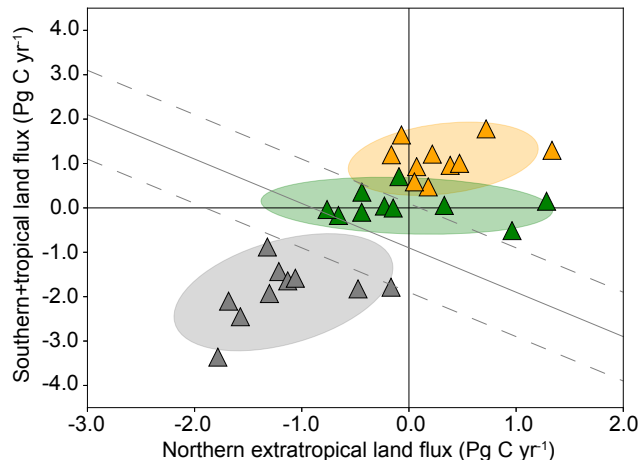


(a)

El Niño years (02, 03, 04, 05, 06, 09)

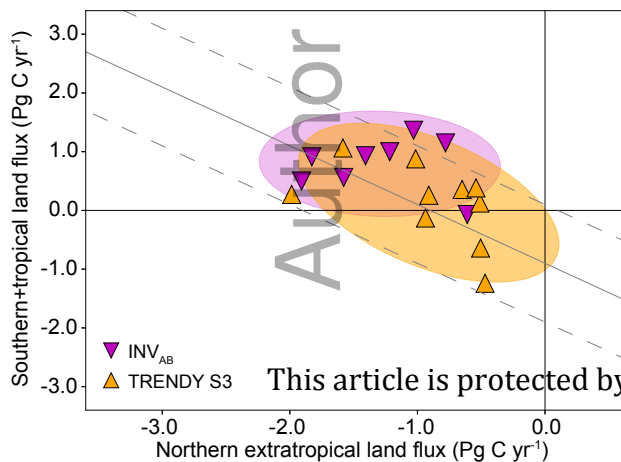


La Niña years (00, 07, 08)

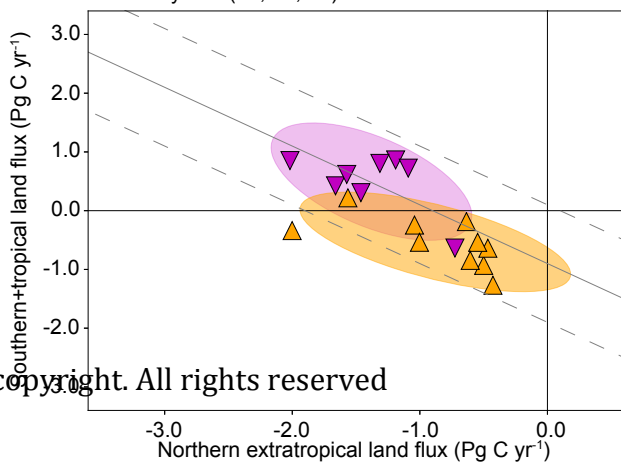


(b)

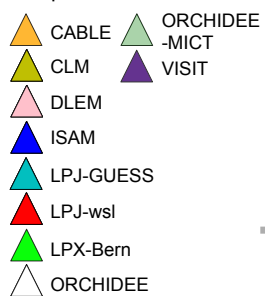
El Niño years (02, 03, 04, 05, 06, 09)



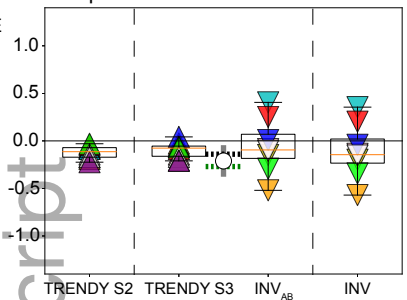
La Niña years (00, 07, 08)



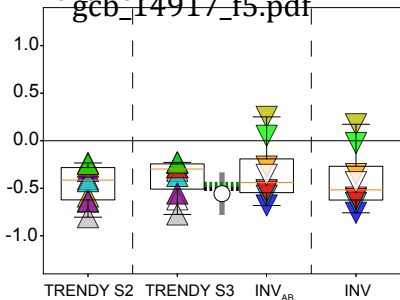
Biosphere model



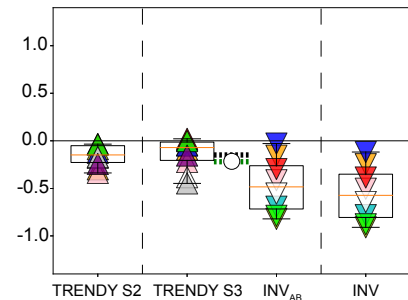
Europe



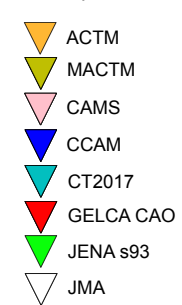
Boreal Asia



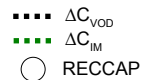
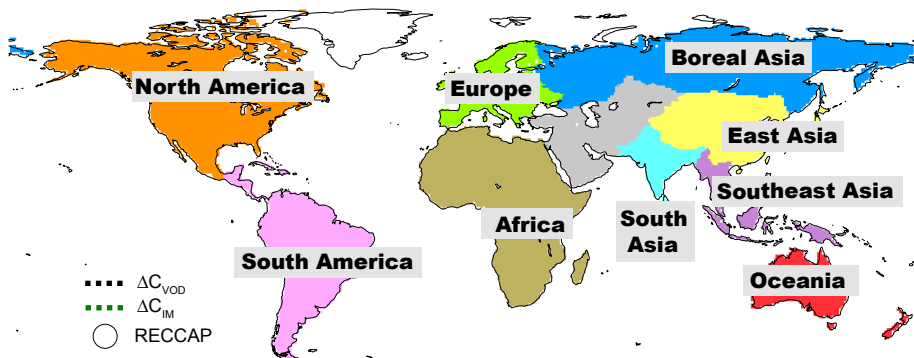
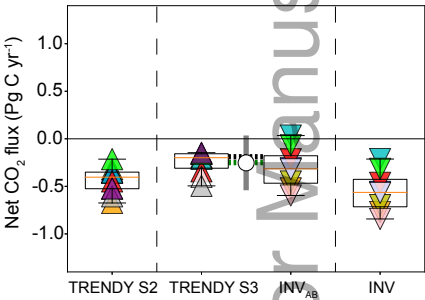
East Asia



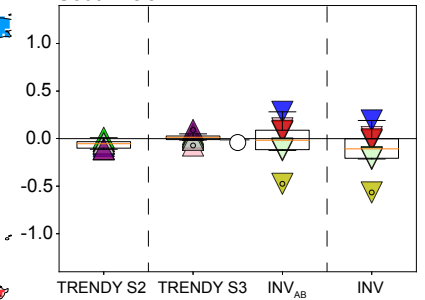
Atmospheric Inversion



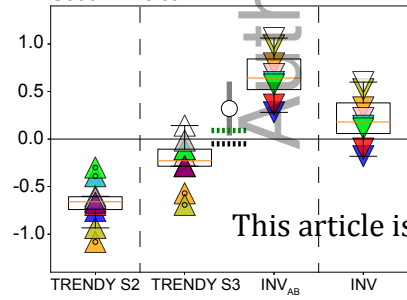
North America



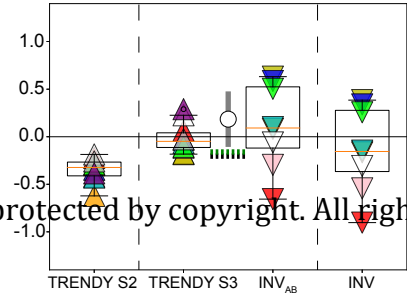
South Asia



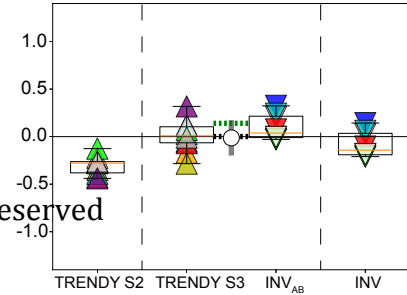
South America



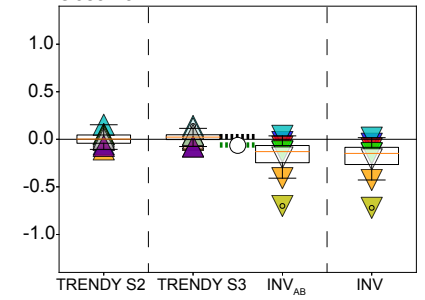
Africa



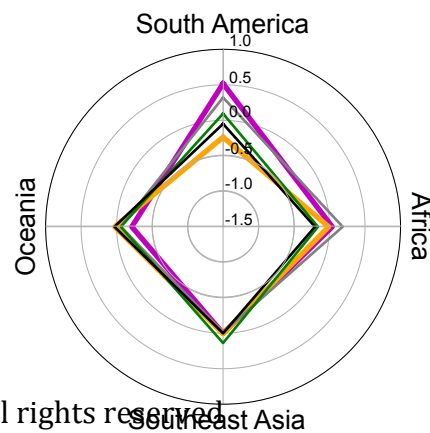
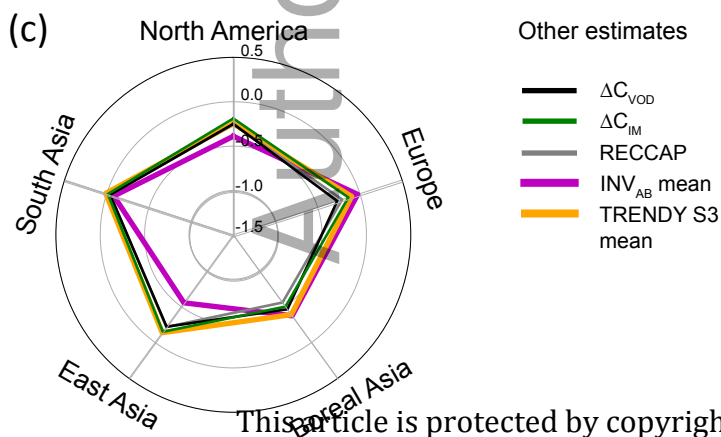
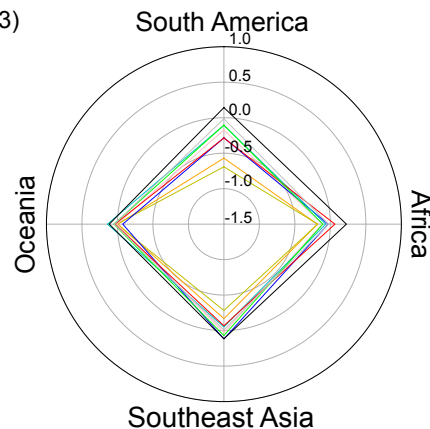
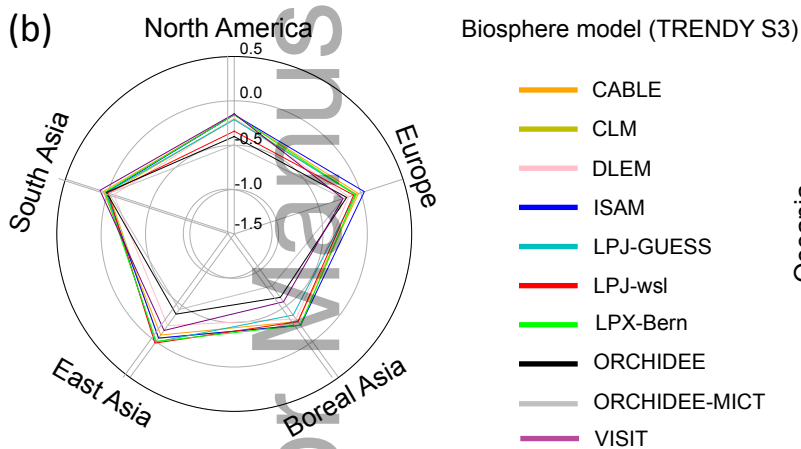
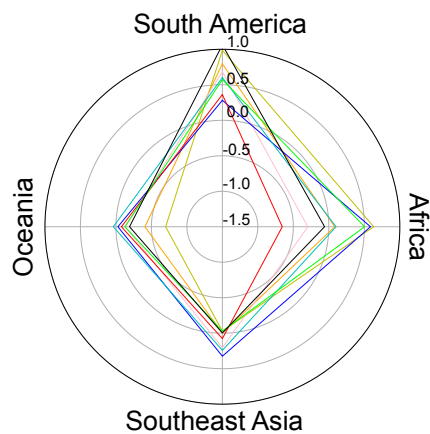
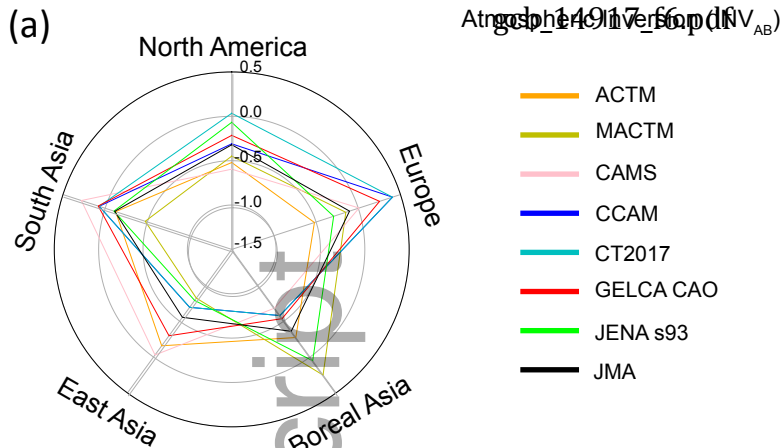
Southeast Asia



Oceania



This article is protected by copyright. All rights reserved



This article is protected by copyright. All rights reserved.

Northern extratropical lands

Southern+Tropical lands